NASA CR-114416
AVAILABLE TO
THE PUBLIC

INVESTIGATION OF LINE-OF-SIGHT PROPAGATION IN DENSE ATMOSPHERE: PHASE III, PART I

FINAL REPORT

BY

D. A. DE WOLF AND G. S. KAPLAN

NOVEMBER 1971

PREPARED UNDER CONTRACT NO. NAS 2-5310

RCA LABORATORIES
PRINCETON, NEW JERSEY 08540

AMES RESEARCH CENTER
MOFFETT FIELD, CALIFORNIA
NATIONAL AERONAUTICS AND SPACE ADMINISTRATION

Requests for copies of this report should be referred to

National Aeronautics and Space Administration
Office of Scientific and Technical Information
Attention: AFSS-A
Washington, D.C. 20546

1. Report No.	2. Government Accession No.	3. Recipient's Catalog No.
Phase III, Part 1 Final Rep.		

4. Title and Subtitle	5. Report Date
Investigation of Line-Of-Sight Propagation in Dense Atmosphere: Phase III, Part 1	November 1971
	6. Performing Organization Code
7. Author(s)	8. Performing Organization Report No.
D. A. de Wolf and G. S. Kaplan	PRRL-71-CR-42
9. Performing Organization Name and Address	10. Work Unit No.
RCA Laboratories Princeton, New Jersey 08540	
	11. Contract or Grant No. NAS 2-5310
	13. Type of Report and Period Covered Final Report May 1971 — Oct. 1971
12. Sponsoring Agency Name and Address	
Ames Research Center Moffett Field, California	14. Sponsoring Agency Code NASA CR-114416

15. Supplementary Notes

16. Abstract

In the current Phase of the study, the investigation of microwave absorption in the 1 to 10 GHz frequency band by the Jovian atmosphere has continued and an estimate of the strength of signal fading at these frequencies due to layers of turbulence in Jupiter's atmosphere is given. (1) The microwave absorption — due to gaseous ammonia as hypothesized in the JPL/Lewis models — is estimated both in terms of a power loss in dB/km, and in total power loss in dB for slant-path communication with a probe at altitudes down to pressures of several tens of atmospheres. The graphs indicate a frequency-squared scaling of the absorption, and appreciable losses (10 dB at 2 GHz) at altitudes where the pressure is several atmospheres (25 atm. for this example). (2) An estimate of turbulence strength is given. This may turn out to be quite crude considering the absence of any relevant data. A planetary scaling law which appears to hold reasonably well for Earth to Venus, is extrapolated to Jupiter. No reasonable modifications of the estimate can alter the conclusion that direct-path fading is negligible for pressure regimes up to 20 atm. Occultation-path fading, although much larger, also appears negligible, unless we have underestimated the strength of turbulence by an order of magnitude.

17. Key Words (Selected by Author(s))	18. Distribution Statement
dense planetary atmosphere propagation ammonia absorption turbulent atmosphere	Available to the public

19. Security Classif. (of this report)	20. Security Classif. (of this page)	21. No. of Pages	22. Price*
Unclassified	Unclassified	42	

*For sale by the Clearinghouse for Federal Scientific and Technical Information, Springfield, Virginia 22151.

Investigation of Line-of-Sight Propagation in Dense Atmosphere: Phase III, Part I

by

D. A. de Wolf and G. S. Kaplan
RCA Laboratories
Princeton, New Jersey

SUMMARY AND CONCLUSIONS

In the current Phase of the study, the investigation of microwave absorption in the 1 to 10 GHz frequency band by the Jovian atmosphere has continued, and an estimate of the strength of signal fading at these frequencies due to layers of turbulence in Jupiter's atmosphere is given.

(1) The microwave absorption — due to gaseous ammonia as hypothesized in the JPL/Lewis models — is estimated both in terms of a power loss in dB/km, and in total power loss in dB for slant-path communication with a probe at altitudes down to pressures of several tens of atmospheres. The graphs indicate a frequency-squared scaling of the absorption and appreciable losses (10 dB at 2 GHz) at altitudes where the pressure is several atmospheres (25 atm for this example).

(2) An estimate of turbulence strength is given. This may turn out to be quite crude considering the absence of any relevant data. A planetary scaling law, which appears to hold reasonably well for Earth to Venus, is extrapolated to Jupiter. No reasonable modifications of the estimate can alter the conclusion that direct-path fading is negligible for pressure regimes up to 20 atm. Occultation-path fading, although much larger, also appears negligible, unless we have underestimated the strength of turbulence by an order of magnitude.

TABLE OF CONTENTS

ILLUSTRATIONS

ILLUSTRATIONS (Cont'd.)

I. ABSORPTION OF ELECTROMAGNETIC WAVES BY THE ATMOSPHERE OF JUPITER

A. INTRODUCTION

Factors which tend to limit communications over a given channel are generally of two broad types: noise introduced by the communications channel, and the effects of the communications channel on the signal itself. The Jovian communications channel, through introduction of amplitude and phase fluctuations, beam spreading due to atmospheric refractive effects, and absorption of energy from the propagating electromagnetic wave, can significantly affect communications capability. It is the purpose of this section to describe our most recent work on the absorptive effects of the Jovian atmosphere. The investigation was initiated in previous phases of this work, and the status at the beginning of the present phase is reported in ref. 1. We will first summarize the main conclusions of our previous work, and then present ensuing results.

The total amount of absorption that a signal will experience in the Jovian atmosphere depends on the atmospheric constituents, their distribution, the operating frequency, and the actual propagation path. In other words, atmospheric, operational, and geometric parameters all influence the total absorption along a given path. Therefore, calculation of the absorption of a signal propagating in the atmosphere of Jupiter is performed in three distinct steps.

First is the determination of the atmospheric composition of Jupiter and its distribution. Second is the determination of the absorption coefficient (a function of the atmospheric parameters). Third is the combining of the information gleaned from the first two tasks and its application to a specific path of interest.

B. ATMOSPHERIC COMPOSITION OF JUPITER

There have been many models proposed for the atmosphere of Jupiter. Some of these have been referenced in the previous Phase II report. The models assumed in this effort are based on the work of Lewis (MIT) and Divine (JPL). Actually, we consider three Lewis/JPL model atmospheres termed *cool dense*, *nominal*, and *warm extended*, and they are presented in Tables 1, 2, and 3. A more complete discussion of the models may be found in ref. 2. For a "broad brush" description, it should be noted that at the same value of pressure, the cool dense model has the lowest value of temperature of all three models whereas the warm extended model would have the highest value of temperature, and (as expected) the nominal-model temperature is in between the others. Note that the zero of the reference height is arbitrarily chosen at the 1-atm pressure point and is not to be considered the top of the cloud layer. In all three models, the principal constituents are hydrogen and helium. The refractivity for the three models is shown in Fig. 1.

Table 1

Gas Abundance for Cool, Dense Model Jupiter Atmosphere

$P_{H2} \approx .69\,P \qquad P_{He} \approx .31\,P$

Z	T	P	P_{NH_3}	P_{H_2S}	P_{H_2O}	P_{CH_4}
km	deg K	atm	atm	atm	atm	atm
+25	108	.16	-	-	-	2.3×10^{-4}
+20	108	.24	-	-	-	3.5×10^{-4}
+15	117	.35	-	-	-	4.8×10^{-4}
+10	126	.48	-	-	-	7.0×10^{-4}
+5	135	.70	1.0×10^{-5}	-	-	1.0×10^{-3}
0	144	1.0	6.0×10^{-5}	-	-	1.4×10^{-3}
-5	153	1.3	4.0×10^{-4}	-	-	1.8×10^{-3}
-10	161	1.7	5.0×10^{-4}	-	-	2.4×10^{-3}
-15	169	2.3	6.0×10^{-4}	-	-	3.2×10^{-3}
-20	179	3.0	7.5×10^{-4}	-	-	4.2×10^{-3}
-25	187	3.6	9.3×10^{-4}	1.0×10^{-5}	-	5.2×10^{-3}
-30	196	4.4	1.15×10^{-3}	3.0×10^{-5}	-	6.3×10^{-3}
-35	204	5.3	1.4×10^{-3}	1.0×10^{-4}	-	7.5×10^{-3}
-40	213	6.4	1.8×10^{-3}	3.0×10^{-4}	1.0×10^{-5}	9.0×10^{-3}
-45	222	7.8	2.2×10^{-3}	3.6×10^{-4}	2.8×10^{-5}	1.1×10^{-2}
-50	230	9.5	2.8×10^{-3}	4.6×10^{-4}	9.0×10^{-5}	1.3×10^{-2}
-55	239	11.5	3.5×10^{-3}	6.0×10^{-4}	2.8×10^{-4}	1.5×10^{-2}
-60	248	13.9	4.3×10^{-3}	7.1×10^{-4}	9.0×10^{-4}	1.8×10^{-2}
-65	257	16.8	5.4×10^{-3}	9.0×10^{-4}	1.5×10^{-3}	2.2×10^{-2}
-70	266	20.0	6.6×10^{-3}	1.1×10^{-3}	3.0×10^{-3}	2.6×10^{-2}
-75	275	25.0	8.2×10^{-3}	1.4×10^{-3}	5.5×10^{-3}	3.4×10^{-2}
-80	284	30.0	1.0×10^{-2}	1.8×10^{-3}	1.0×10^{-2}	4.2×10^{-2}
-85	293	36.0	1.2×10^{-2}	2.3×10^{-3}	1.8×10^{-2}	5.3×10^{-2}
-90	302	44.0	1.5×10^{-2}	2.8×10^{-3}	3.3×10^{-2}	6.4×10^{-2}
-95	311	53.0	1.8×10^{-2}	3.4×10^{-3}	6.4×10^{-2}	7.5×10^{-2}
-100	320	65.0	2.2×10^{-2}	4.0×10^{-3}	1.1×10^{-1}	8.6×10^{-2}
-105	329	78.0	2.4×10^{-2}	4.6×10^{-3}	1.7×10^{-1}	9.7×10^{-2}
-120	348	92.0	3.2×10^{-2}	5.3×10^{-3}	1.9×10^{-1}	1.1×10^{-1}
-130	367	108.0	4.0×10^{-2}	6.6×10^{-3}	2.2×10^{-1}	1.3×10^{-1}
-140	385	136.0	5.0×10^{-2}	8.3×10^{-3}	2.8×10^{-1}	1.7×10^{-1}
-150	404	171.0	5.5×10^{-2}	9.1×10^{-3}	3.5×10^{-1}	2.1×10^{-1}
-160	423	215.0	6.7×10^{-2}	1.1×10^{-2}	4.4×10^{-1}	2.6×10^{-1}
-170	441	270.0	8.5×10^{-2}	1.4×10^{-2}	5.5×10^{-1}	3.3×10^{-1}
-175	450	300.0	1.0×10^{-1}	1.6×10^{-2}	6.1×10^{-1}	3.7×10^{-1}
-180	459	333.0	1.1×10^{-1}	1.7×10^{-2}	6.7×10^{-1}	4.1×10^{-1}
-185	468	375.0	1.2×10^{-1}	1.9×10^{-2}	7.5×10^{-1}	4.5×10^{-1}
-190	477	422.0	1.4×10^{-1}	2.2×10^{-2}	8.5×10^{-1}	5.1×10^{-1}
-195	486	471.0	1.6×10^{-1}	2.6×10^{-2}	9.5×10^{-1}	5.7×10^{-1}
-200	495	530.0	1.8×10^{-1}	3.0×10^{-2}	1.1×10^{-1}	6.6×10^{-1}

Table 2

Gas Abundance for Nominal Model Jupiter Atmosphere

$P_{H2} \approx .87\,P \qquad P_{He} \approx .13\,P$

Z	T	P	P_{NH_3}	P_{H_2S}	P_{H_2O}	P_{CH_4}
km	deg K	atm	atm	atm	atm	atm
+25	125	.30	-	-	-	2.0×10^{-4}
+20	136	.40	1.0×10^{-5}	-	-	3.0×10^{-4}
+15	147	.55	1.0×10^{-4}	-	-	4.0×10^{-4}
+10	158	.70	1.2×10^{-4}	-	-	5.0×10^{-4}
+5	169	.85	1.4×10^{-4}	-	-	6.0×10^{-4}
0	180	1.00	1.7×10^{-4}	1.0×10^{-5}	-	7.0×10^{-4}
-5	191	1.15	1.9×10^{-4}	2.0×10^{-5}	-	8.0×10^{-4}
-10	202	1.30	2.2×10^{-4}	4.4×10^{-5}	-	9.0×10^{-4}
-15	212	1.45	2.5×10^{-4}	5.0×10^{-5}	1.0×10^{-5}	1.0×10^{-3}
-20	223	1.60	2.7×10^{-4}	5.6×10^{-5}	6.0×10^{-5}	1.1×10^{-3}
-25	234	1.80	3.1×10^{-4}	6.2×10^{-5}	2.0×10^{-4}	1.3×10^{-3}
-30	244	2.10	3.6×10^{-4}	7.2×10^{-5}	8.0×10^{-4}	1.5×10^{-3}
-35	255	2.40	4.1×10^{-4}	8.2×10^{-5}	1.5×10^{-3}	1.7×10^{-3}
-40	265	2.80	4.8×10^{-4}	9.6×10^{-5}	2.2×10^{-3}	1.9×10^{-3}
-45	276	3.2	5.4×10^{-4}	1.1×10^{-4}	3.8×10^{-3}	2.9×10^{-3}
-50	286	3.7	6.3×10^{-4}	1.3×10^{-4}	4.5×10^{-3}	2.6×10^{-3}
-55	297	4.3	7.3×10^{-4}	1.5×10^{-4}	5.0×10^{-3}	3.0×10^{-3}
-60	307	5.0	8.5×10^{-4}	1.7×10^{-4}	6.0×10^{-3}	3.5×10^{-3}
-65	317	5.8	9.7×10^{-4}	1.9×10^{-4}	7.0×10^{-3}	4.1×10^{-3}
-70	327	6.6	1.1×10^{-3}	2.1×10^{-4}	8.0×10^{-3}	4.7×10^{-3}
-80	347	8.4	1.4×10^{-3}	2.7×10^{-4}	1.0×10^{-2}	6.0×10^{-3}
-90	366	10.3	1.7×10^{-3}	3.4×10^{-4}	1.2×10^{-2}	7.0×10^{-3}
-100	385	12.0	2.0×10^{-3}	4.0×10^{-4}	1.4×10^{-2}	8.0×10^{-3}
-110	403	14.0	2.3×10^{-3}	4.6×10^{-4}	1.6×10^{-2}	9.0×10^{-3}
-120	421	16.0	2.7×10^{-3}	5.3×10^{-4}	1.9×10^{-2}	1.1×10^{-2}
-130	439	18.0	3.1×10^{-3}	6.0×10^{-4}	2.2×10^{-2}	1.3×10^{-2}

Table 3

Gas Abundance for Warm, Extended Model Jupiter Atmosphere

$P_{H2} \approx .94\,P \qquad P_{He} \approx .06\,P$

Z	T	P	P_{NH_3}	P_{H_2S}	P_{H_2O}	P_{CH_4}
km	deg K	atm	atm	atm	atm	atm
+50	120	.20	-	-	-	7.0×10^{-5}
+45	132	.26	1.0×10^{-5}	-	-	9.0×10^{-5}
+40	144	.32	2.7×10^{-5}	-	-	1.1×10^{-4}
+35	155	.39	3.2×10^{-5}	-	-	1.3×10^{-4}
+30	167	.46	3.7×10^{-5}	-	-	1.5×10^{-4}
+25	179	.54	4.3×10^{-5}	3.0×10^{-6}	-	1.7×10^{-4}
+20	191	.62	5.0×10^{-5}	1.0×10^{-5}	-	2.0×10^{-4}
+15	202	.71	5.9×10^{-5}	1.2×10^{-5}	-	2.4×10^{-4}
+10	214	.80	7.0×10^{-5}	1.4×10^{-5}	1.0×10^{-5}	2.8×10^{-4}
+5	226	.90	7.9×10^{-5}	1.6×10^{-5}	6.0×10^{-5}	3.2×10^{-4}
0	238	1.00	8.8×10^{-5}	1.8×10^{-5}	3.0×10^{-4}	3.5×10^{-4}
-5	249	1.11	9.8×10^{-5}	1.9×10^{-5}	6.5×10^{-4}	3.9×10^{-4}
-10	261	1.23	1.1×10^{-4}	2.2×10^{-5}	7.3×10^{-4}	4.3×10^{-4}
-15	273	1.36	1.2×10^{-4}	2.4×10^{-5}	8.1×10^{-4}	4.8×10^{-4}
-20	285	1.51	1.3×10^{-4}	2.7×10^{-5}	9.0×10^{-4}	5.3×10^{-4}
-25	297	1.68	1.5×10^{-4}	3.0×10^{-5}	1.0×10^{-3}	5.9×10^{-4}
-30	309	1.87	1.6×10^{-4}	3.2×10^{-5}	1.1×10^{-3}	6.5×10^{-4}
-35	321	2.08	1.7×10^{-4}	3.5×10^{-5}	1.2×10^{-3}	7.3×10^{-4}
-40	333	2.31	1.9×10^{-4}	3.9×10^{-5}	1.3×10^{-3}	8.1×10^{-4}
-45	345	2.56	2.1×10^{-4}	4.3×10^{-5}	1.4×10^{-3}	8.9×10^{-4}
-50	357	2.82	2.4×10^{-4}	4.8×10^{-5}	1.6×10^{-3}	9.7×10^{-4}
-55	369	3.10	2.6×10^{-4}	5.3×10^{-5}	1.8×10^{-3}	1.0×10^{-3}
-60	381	3.40	2.9×10^{-4}	5.9×10^{-5}	2.0×10^{-3}	1.2×10^{-3}
-65	393	3.72	3.2×10^{-4}	6.5×10^{-5}	2.2×10^{-3}	1.3×10^{-3}
-70	405	4.06	3.5×10^{-4}	7.1×10^{-5}	2.4×10^{-3}	1.4×10^{-3}
-75	417	4.45	3.8×10^{-4}	7.7×10^{-5}	2.6×10^{-3}	1.5×10^{-3}
-80	429	4.87	4.1×10^{-4}	8.2×10^{-5}	2.8×10^{-3}	1.7×10^{-3}

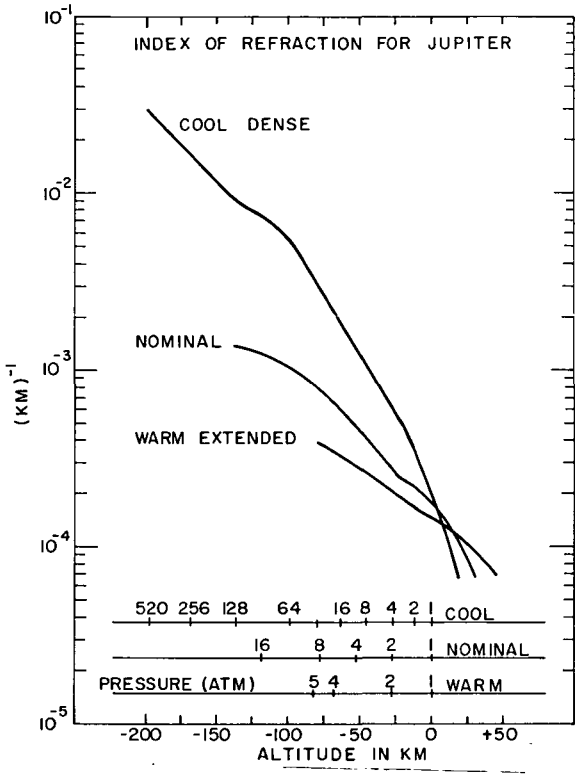

Figure 1.

Refractivity of Jupiter's atmosphere for the cool dense, nominal, and warm extended models proposed by Lewis/JPL.

C. ABSORPTION COEFFICIENT

An absorptive medium extracts energy from an electromagnetic wave, with the remaining electromagnetic power per unit solid angle (or radiance) decaying exponentially along the path. The rate at which the power decays is measured by the absorption coefficient which is usually expressed as nepers per meter. Due to the large distances involved in planetary geometries, it is more convenient to express the absorption coefficient in decibels per km. Conversion between the two systems is: absorption coefficient (dB/km) = 4.34×10^3 absorption (nepers/m).

Although there are a number of constituents shown in the Lewis/JPL model atmospheres, our previous studies show that the dominant absorber is ammonia at the frequencies of interest in this study (X band and lower).

Absorption by ammonia occurs when the incoming electromagnetic wave excites the NH_3 molecule to a higher energy state. The molecular structure of NH_3 is a pyramid (classified as a symmetric top) with the three hydrogen atoms forming the base of the pyramid. Excitation of the molecule so that the nitrogen changes position (inversion) above or below the basal plane leads to an absorption spectrum. This inversion spectrum is extremely complex with a large number (over 60) of spectral lines existing between 17 and 40 GHz. In addition, collisions between molecules of the same or differing species broadens the spectral "lines" so that their influence as absorbers becomes important even far from resonance. Under pressure-induced collisions, line broadening occurs and the various absorbing "lines" overlap.

For a single inversion line, the absorption coefficient (α) is given in Eq. (1). This result was obtained by Ben-Reuven and it differs from the previous expressions given by Van-Vleck and Weisskopf.

$$\alpha_{ij}(\nu) = \frac{\pi f_i |\mu_{ij}|^2}{3ckT\epsilon_o} N\nu^2 \; F_i(\gamma_{ij}, \zeta_{ij}, \nu_{ij}, \nu) \tag{1}$$

$$F_i = \frac{2(\gamma_{ij} - \zeta_{ij})\nu^2 + 2(\gamma_{ij} + \zeta_{ij})\left[(\nu_{ij})^2 + \gamma_{ij}^2 - \zeta_{ij}^2\right]}{\left[(\nu_{ij})^2 - \nu^2 + \gamma_{ij}^2 - \zeta_{ij}^2\right]^2 + 4\nu^2\gamma_{ij}^2}$$

and

α_{ij} is the absorption coefficient for a single transition (nepers/m)

μ_{ij} is the dipole moment matrix element (coulomb/m)

f_i is the fraction of molecules in the lower state

c is the velocity of light 3×10^8 m/sec

ϵ_o is 8.85×10^{-12} farads/m

N is the number of ammonia molecules per unit volume (m^{-3})

ν is the operating frequency

μ_{ij} is resonance frequency

γ_{ij} and ζ_{ij} are collision induced terms (Hz)

After summing over all the inversion lines we obtain Eq. (2)

$$\alpha(\nu) = \sum \alpha_i(\nu) = \frac{\pi N\nu^2}{3ckT_o} \sum f_i |\mu_{ij}|^2 \, Fi(\gamma_{ij}, \zeta_{ij}, \nu_{ij}, \nu) \tag{2}$$

Since the sum is tedious and complex for all 66 inversion lines, it was argued in the previous report that the complex sum can be replaced by the expression shown in Eq. (3).

$$\alpha(\nu) = \sum \alpha_i = \frac{\pi}{3ckT_o} N\nu^2 \, F(\gamma, \zeta, \nu_o, \nu) \, f|\mu_{ij}|^2 \tag{3}$$

where γ, ζ and ν_o represent average values for the parameters.

After substitution of $N = P_{NH_3}/kT$ into Eq. (3), where P_{NH_3} is the partial pressure of ammonia, and numerically evaluating the remaining constants, Eq. (4) is obtained

$$\alpha(\nu) = \frac{2.6 \times 10^{-3} P_{NH_3} \nu^2}{T^2} \frac{2(\gamma-\zeta)^2\nu^2 + 2(\gamma+\zeta)\left[\nu_o^2 + \gamma^2 - \zeta^2\right]}{\left[\nu_o^2 - \nu^2 + \gamma^2 - \zeta^2\right]^2 + 4\nu^2\gamma^2} \quad (4)$$

α is given in nepers/m when the pressure is expressed in Torr, temperature in degrees Kelvin, and all frequencies in MHz.

In the above expression γ and ζ are pressure-induced collision frequency terms and are given by Eq. (5)

$$\begin{aligned} \gamma &= a_{NH_3} P_{NH_3} + a_{H_2} P_{H_2} + a_{He} P_{He} \\ \zeta &= b_{NH_3} P_{NH_3} + b_{H_2} P_{H_2} + b_{He} P_{He} \end{aligned} \quad (5)$$

where the pressures are all partial pressures and the a's and b's are functions of temperature. These values were determined experimentally and reported in the previous report. The results are shown in Eq. (6).

$$\begin{aligned} a_{NH_3} &= 21.4 \left(\frac{300}{T}\right) \\ b_{NH_3} &= 14.1 \left(\frac{300}{T}\right) \\ a_{H_2} &= 2.5 \left(\frac{300}{T}\right)^{.6} \\ b_{H_2} &= 1.5 \left(\frac{300}{T}\right)^{.6} \\ a_{He} &= 0.8 \left(\frac{300}{T}\right)^{.7} \\ b_{He} &= 0.4 \left(\frac{300}{T}\right)^{.7} \end{aligned} \quad (6)$$

Note that a and b have the dimensions of MHz per Torr and describe pressure-induced collision frequencies for ammonia broadened with either ammonia, hydrogen, or helium.

The absorption coefficients may be found by substitution into Eqs. (5) and (6) of the inputs from the Lewis/JPL models namely, temperature, the partial pressures of ammonia, hydrogen and helium, and the operating frequencies of interest. They are shown plotted vs. altitude in Figs. 2, 4, and 6, and vs. pressure in Figs. 3, 5, and 7. (Note that the zero km reference altitude is defined at 1-atm pressure and that negative altitudes are closer to the center of the planet.)

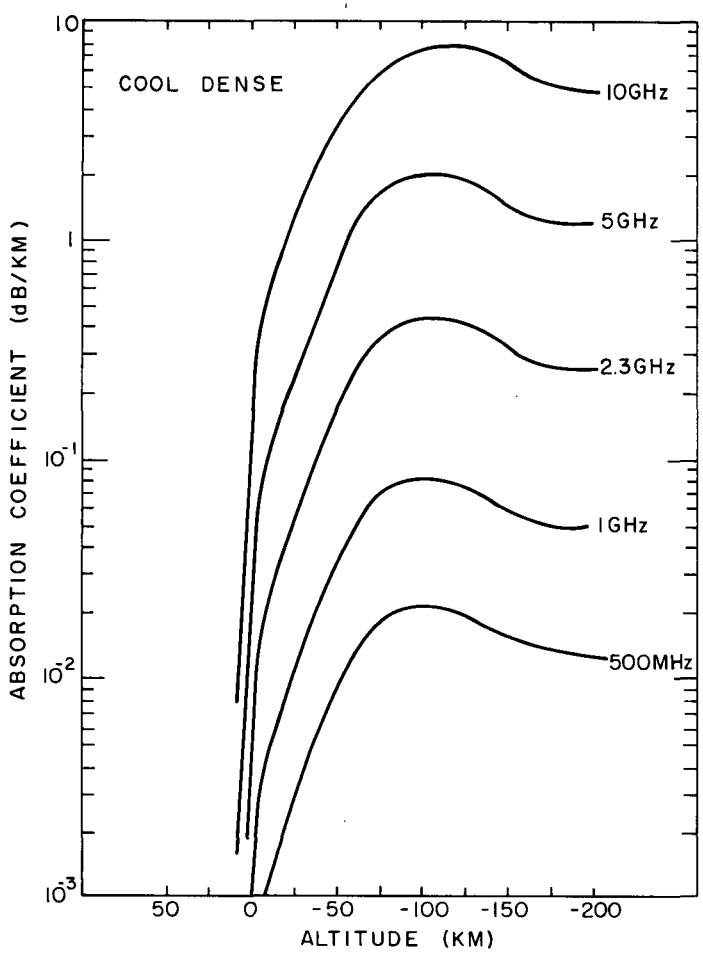

Figure 2. Absorption coefficient vs. altitude for the cool dense model Jovian atmosphere proposed by Lewis/JPL.

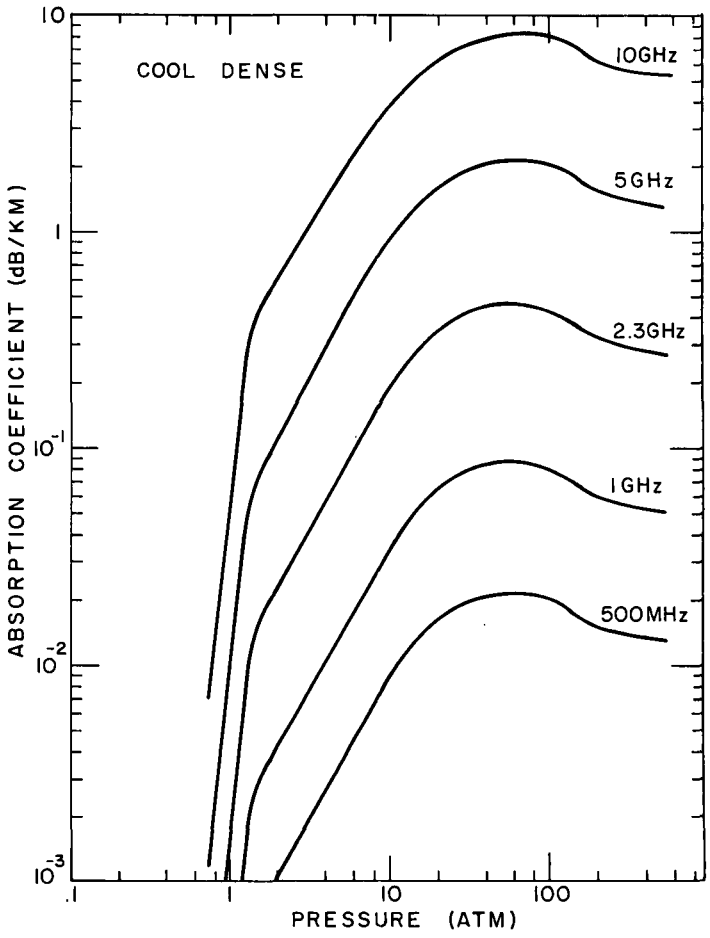

Figure 3. Absorption coefficient vs. pressure for the cool dense model Jovian atmosphere proposed by Lewis/JPL.

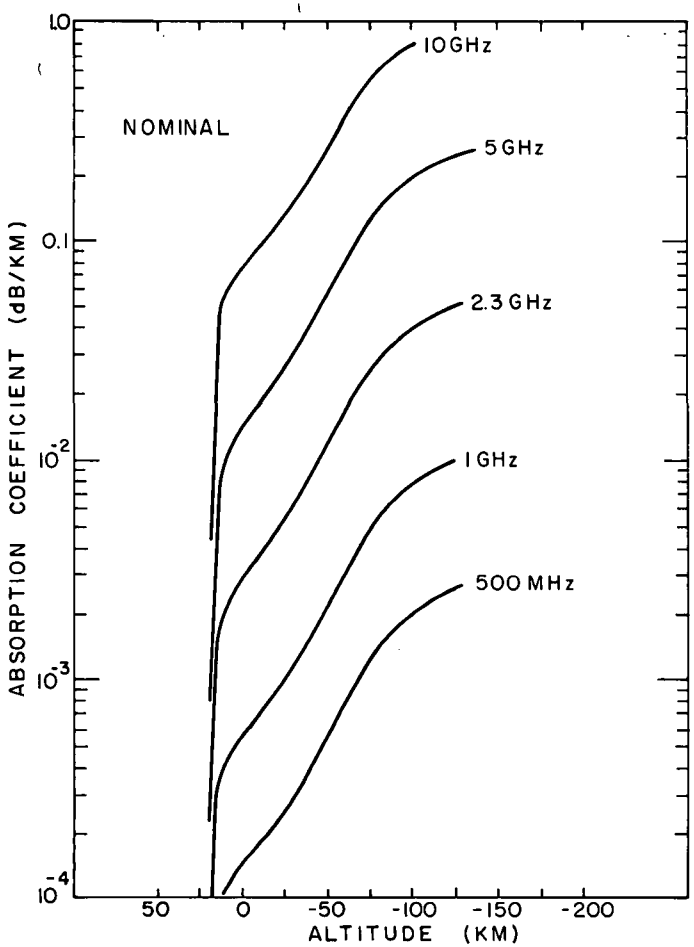

Figure 4. Absorption coefficient vs. altitude for the nominal model Jovian atmosphere proposed by Lewis/JPL.

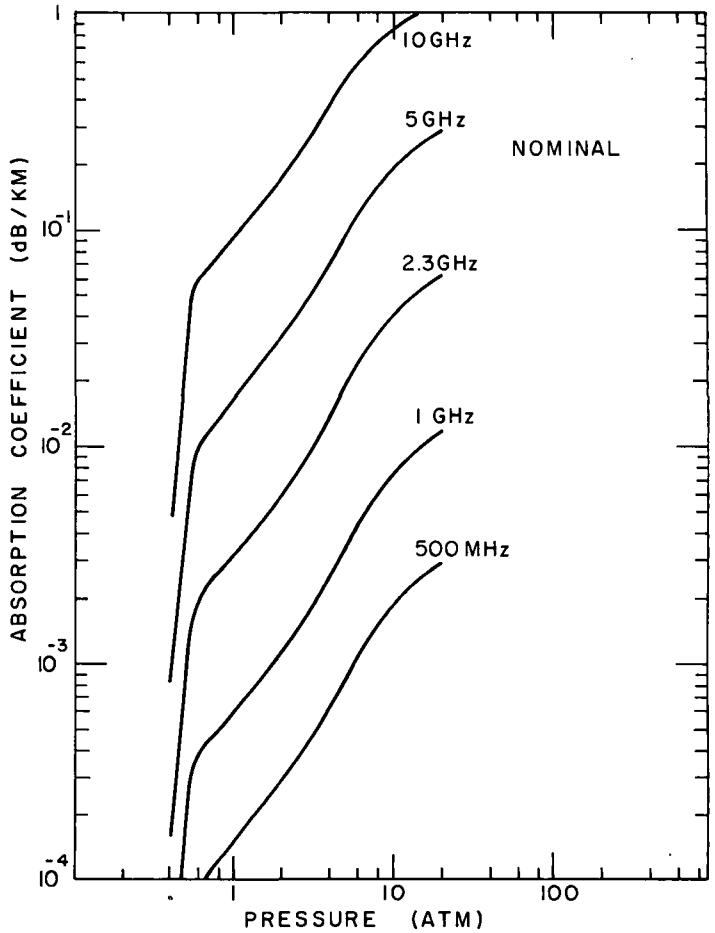

Figure 5. Absorption coefficient vs. pressure for the nominal model Jovian atmosphere proposed by Lewis/JPL.

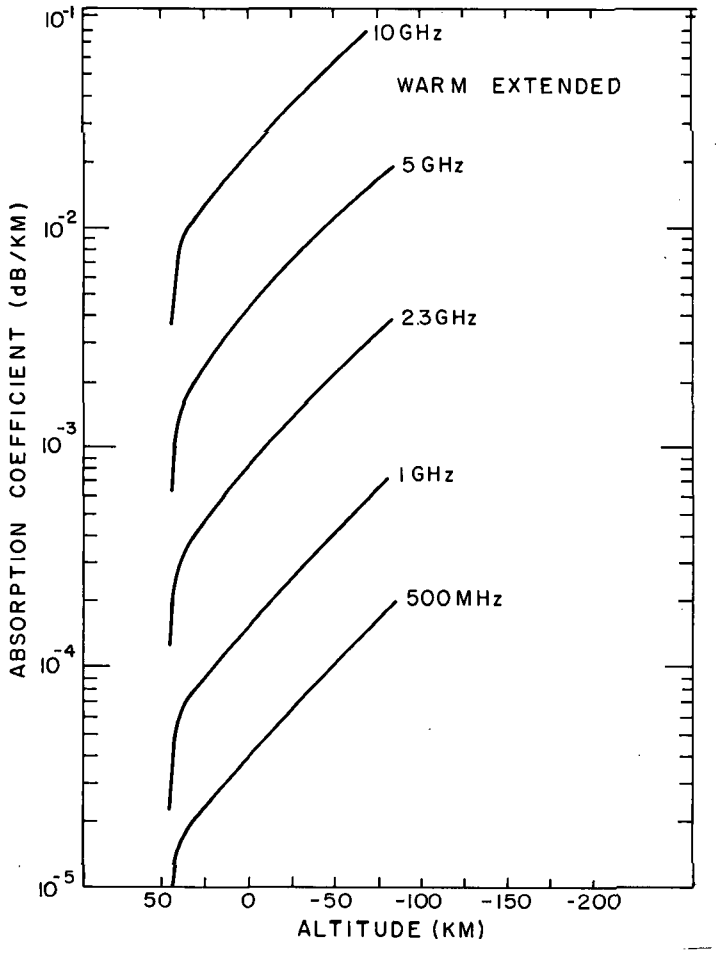

Figure 6. Absorption coefficient vs. altitude for the warm extended model Jovian atmosphere proposed by Lewis/JPL.

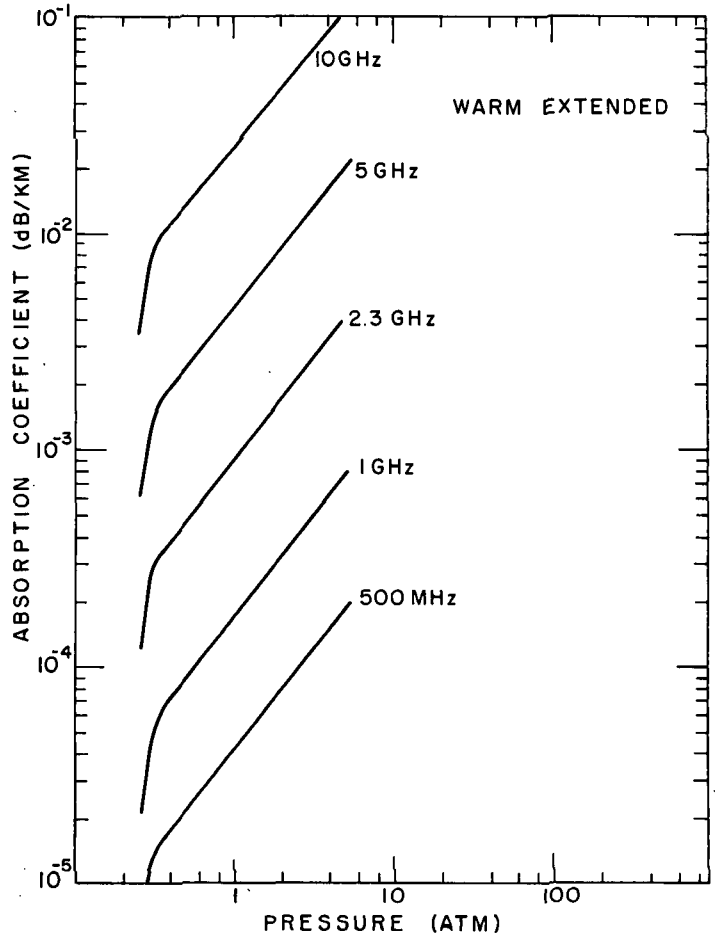

Figure 7. Absorption coefficient vs. pressure for the warm extended model Jovian atmosphere proposed by Lewis/JPL.

The cool dense model has the highest absorption coefficient (at the same pressure) of all three models for pressures greater than about one atmosphere. The warm extended model has the lowest absorption coefficient while the nominal model falls in between the other two. This trend exists because at the same value of total pressure, the ammonia partial pressure is somewhat higher for the cool dense model and, just as important, the temperature is lower. Referring to Eqs. (4)—(6) we note the following limiting conditions for the absorption coefficient at low pressures

$$\alpha \approx \text{constant} \frac{\nu^2 P_{NH_3} P}{T^{2.6}} \tag{7}$$

while at high pressures (beyond saturation)

$$\alpha \approx \text{constant} \frac{\nu^2 P_{NH_3}}{T^{1.4} P} \tag{8}$$

Therefore, the temperature does influence the absorption coefficient (especially at the low pressures). Referring to Figs. 2 and 5, we see the absorption coefficient for the cool dense model decreasing with increasing pressure as predicted by the Ben-Reuven formula.

The nominal and warm extended models do not exhibit the decrease in absorption coefficient because the pressures over which these models are defined do not become high enough for this effect to occur.

Figures 8 through 10 show the absorption coefficient plotted vs. frequency. Below 5 GHz the straight line (with slope 2) on the log-log plot indicates that the absorption coefficient scales as the square of the frequency. Above 5 GHz, the absorption coefficient is increasing at a slightly higher rate than frequency squared as the operating frequency becomes closer to the resonant frequency of $\nu_o = 23.4$ GHz.

D. TOTAL ABSORPTION

The total absorption along a given path is found by integration of the absorption coefficient along that path [as shown in Eq. (9)]

$$\text{Total absorption (dB)} = \int_{\text{along path}} \alpha(s)\,ds \tag{9}$$

where α is the absorption coefficient in dB/km and ds, the differential path length, is expressed in km.

The geometry of interest is shown in Fig. 11. A given path is defined by two parameters, the initial starting point as measured from the center of the planet, R_o, (or as measured from the one atmosphere distance Z_o) and the slant angle θ that the path makes with a radial line drawn through the initial starting position. When the slant angle is zero degrees, the path is termed a *direct path* and when the slant angle is 90 degrees, an *occultation path* results. First consider a direct path.

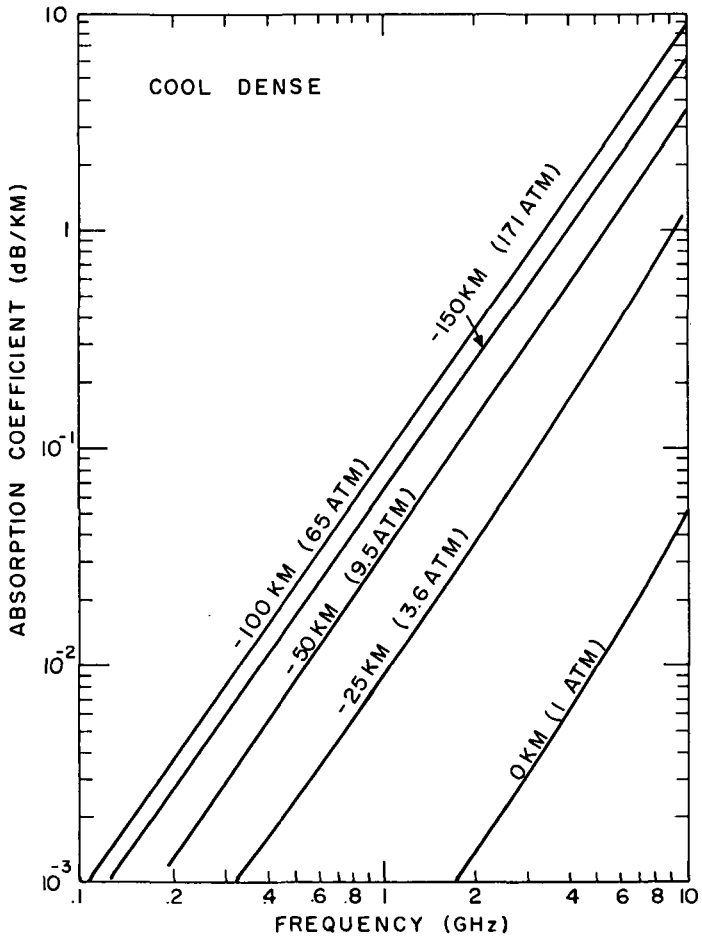

Figure 8. Absorption coefficient vs. frequency (at selected altitudes) for the cool dense model Jovian atmosphere proposed by Lewis/JPL.

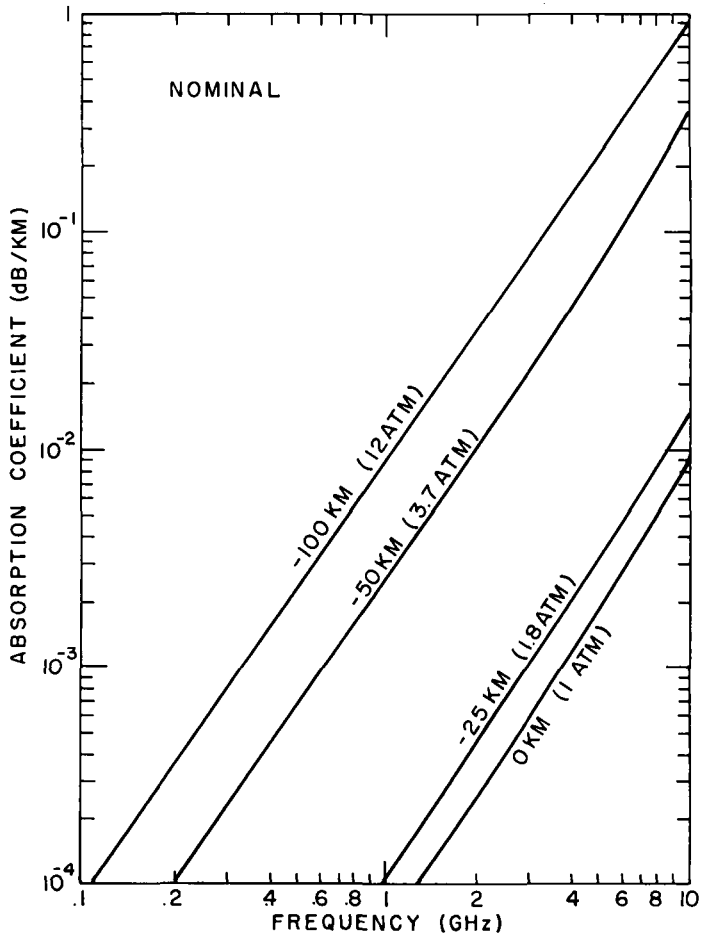

Figure 9. Absorption coefficient vs. frequency (at selected altitudes) for the nominal model Jovian atmosphere proposed by Lewis/JPL.

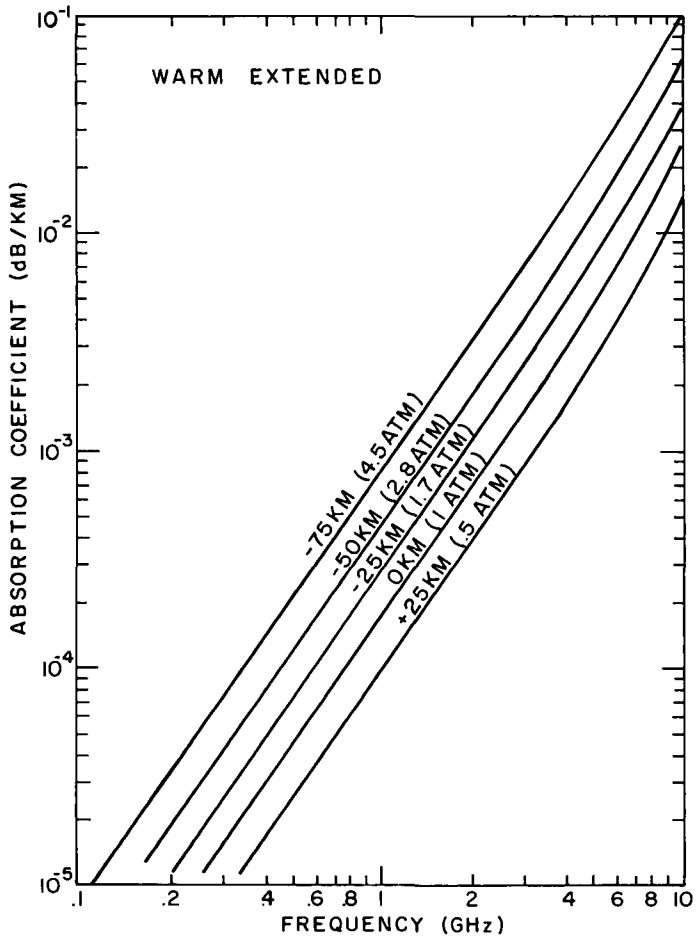

Figure 10. Absorption coefficient vs. frequency (at selected altitudes) for the warm extended model Jovian atmosphere proposed by Lewis/JPL.

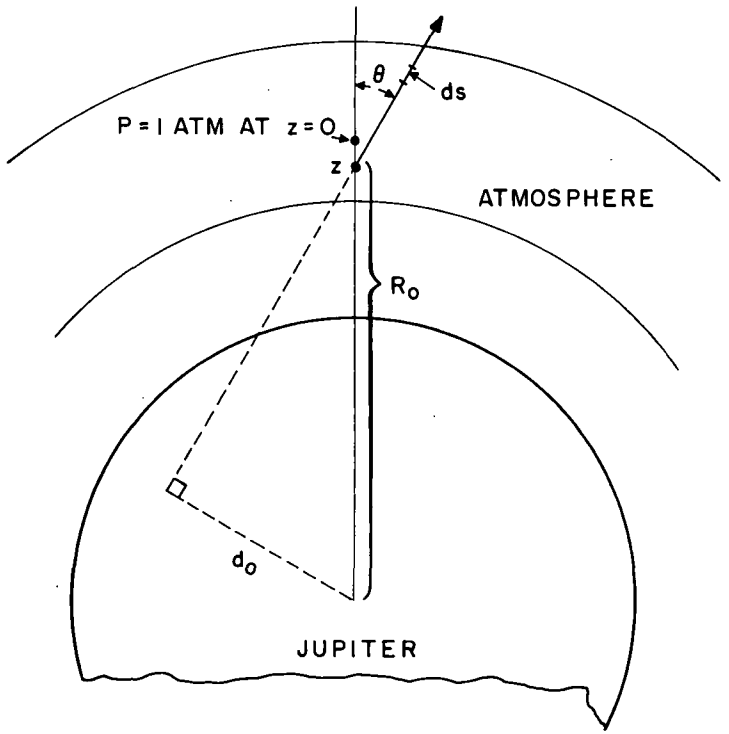

Figure 11. Planetary geometry.

The final position on the path is assumed to be far away from the planet and since most of the absorption occurs over a relatively short distance, the final position is taken to be infinity. A computer program was written to calculate the total absorption along a direct path numerically. To perform this calculation, it was necessary to extend the model atmospheres outside their given altitude (or pressure) range. The extrapolation was performed by assuming that the absorption coefficient decreased further exponentially with increasing altitude. The scale height for the exponential decrease was found from the highest altitude entries for the model atmosphere. In effect, the absorption coefficient for altitudes higher than those defined for the model atmosphere was obtained by essentially drawing a straight line extension on the semi-log plot of absorption coefficient vs. altitude. Then the (residual) absorption due to the extension of the model is easily found to be

$$R = \alpha_{top} \cdot h_{scale}$$

where R is the residual absorption, α_{top} is the absorption coefficient at the highest altitude defined for the model atmosphere, and h_{scale} is the scale height for the absorption coefficient as measured at the highest altitude for the model atmosphere.

The total absorption as a function of penetration depth along a direct path is shown in Figs. 12, 14, and 16, and as a function of maximum probed pressure in Figs. 13, 15, and 17. Note that above a few atmospheres of pressure, the cool dense model produces the most absorption with the nominal model atmosphere producing less absorption and the warm extended atmosphere having the least effect on a signal. Because the absorption coefficient scales as the square of the frequency (Figs. 8 through 10), the total absorption (in dB) also scales as the square of the frequency (below approximately 5 GHz) resulting in the absorption curves at different frequencies being parallel to each other in these log-log-scaled figures. It is clear that substantial absorption (well above one dB) can occur on direct paths especially at the higher frequencies (above 1 GHz) and higher pressures (above 1 atm).

E. EXTENSION OF RESULTS FOR SLANT PATHS

Although the absorption has been evaluated for a direct path, the results may be extended to slant paths as long as the slant path angle θ is not too close to 90 degrees. To apply the absorption results to slant paths the following simple formula (see Appendix I for its derivation) may be used

$$I_{sl} = I_d / \cos\theta \tag{10}$$

where I_d is the total absorption (in dB) along a direct path, I_{sl} is the total absorption (in dB) along a slant path with the same penetration depth as the direct path, and θ is the angle between the slant path and the direct (or radial path).

Equation (10) has the rather simple interpretation that the increased path length traversed on a slant path as compared with a direct path is accounted for by the secant of the angle between the two paths. It is the increased path length which leads to a greater attenuation on slant paths.

The above formula can be applied as long as significant ray bending does not occur and in addition should not be applied for slant path angles greater than approximately 85 degrees (i.e., not to occultation paths).

Therefore the direct-path curves can be used on slant paths if the total absorption given by these figures is increased by the secant of the slant angle.

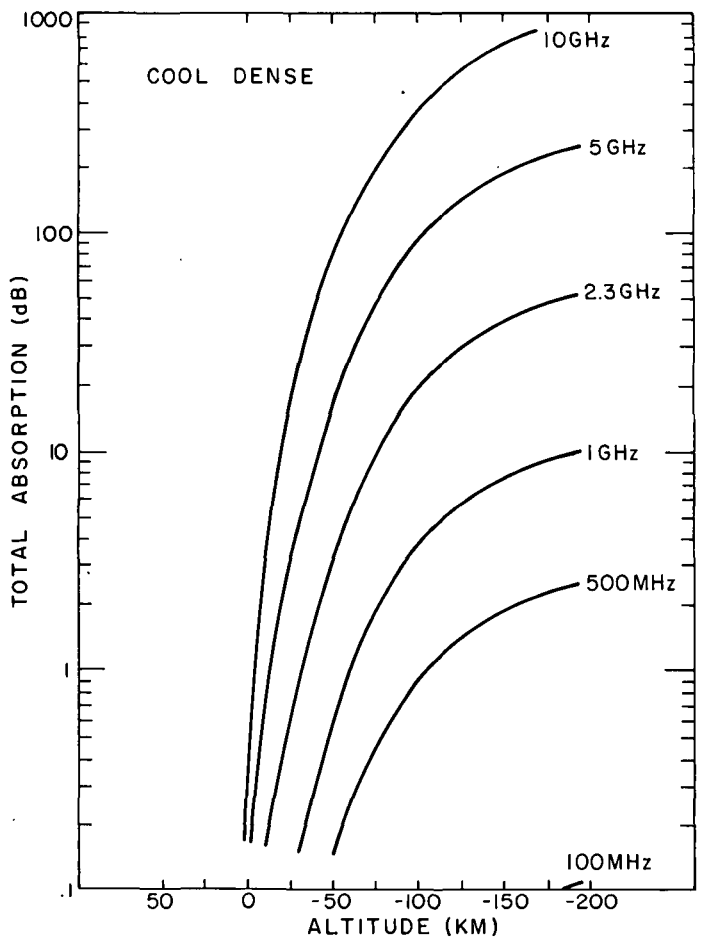

Figure 12. Total absorption vs. altitude for a signal propagating on a direct (radial) path calculated for the cool dense model Jovian atmosphere proposed by Lewis/JPL.

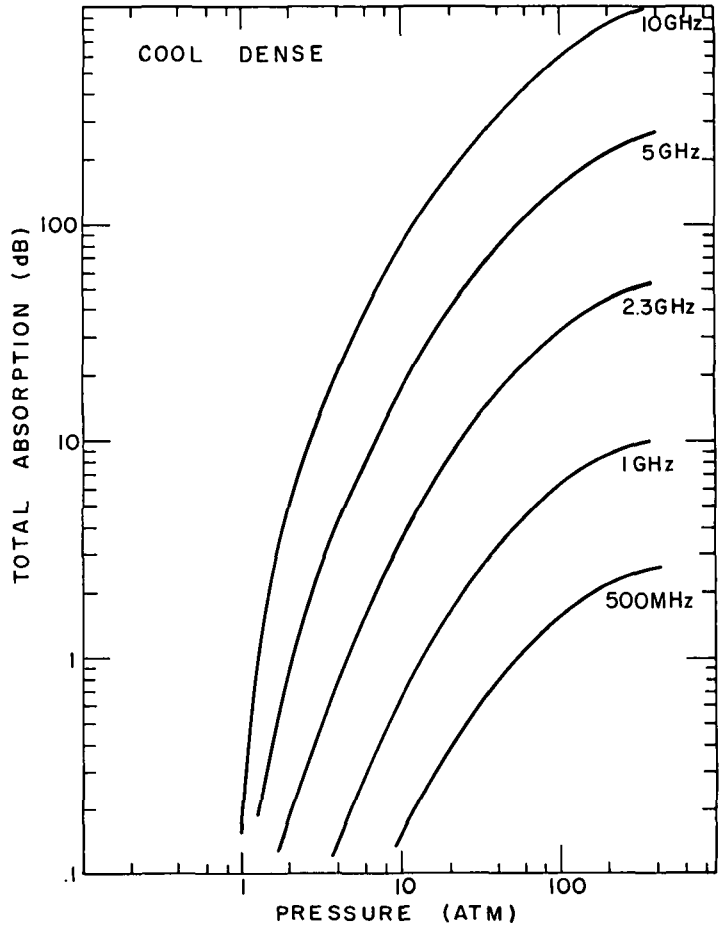

Figure 13. Total absorption vs. pressure for a signal propagating on a direct (radial) path calculated for the cool dense model Jovian atmosphere proposed by Lewis/JPL.

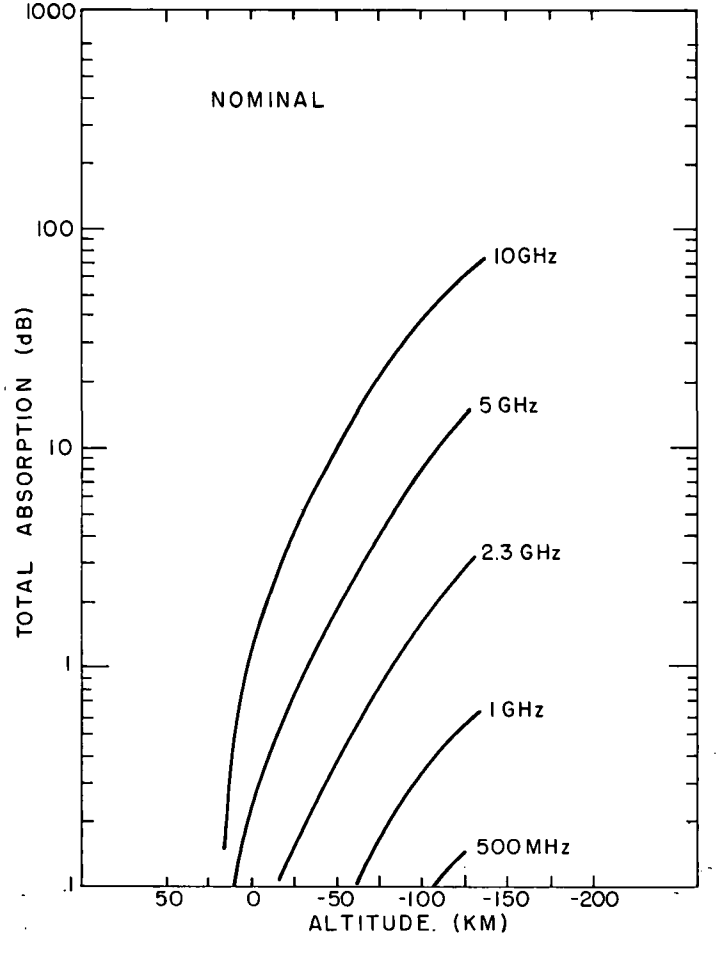

Figure 14. Total absorption vs. altitude for a signal propagating on a direct (radial) path calculated for the nominal model Jovian atmosphere proposed by Lewis/JPL.

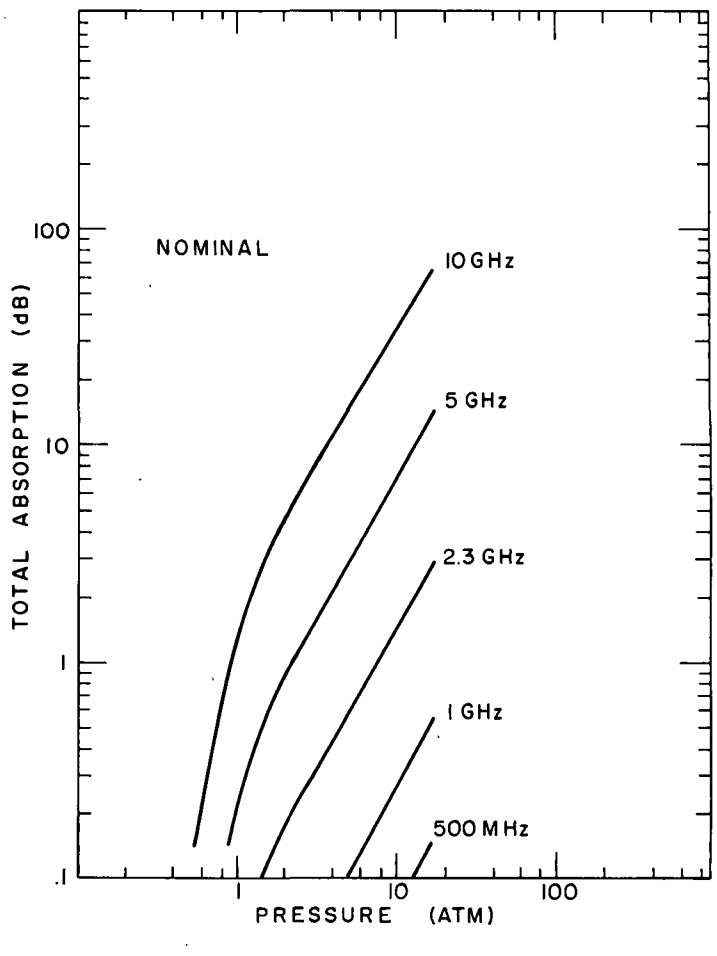

Figure 15. Total absorption vs. pressure for a signal propagating on a direct (radial) path calculated for the nominal model Jovian atmosphere proposed by Lewis/JPL.

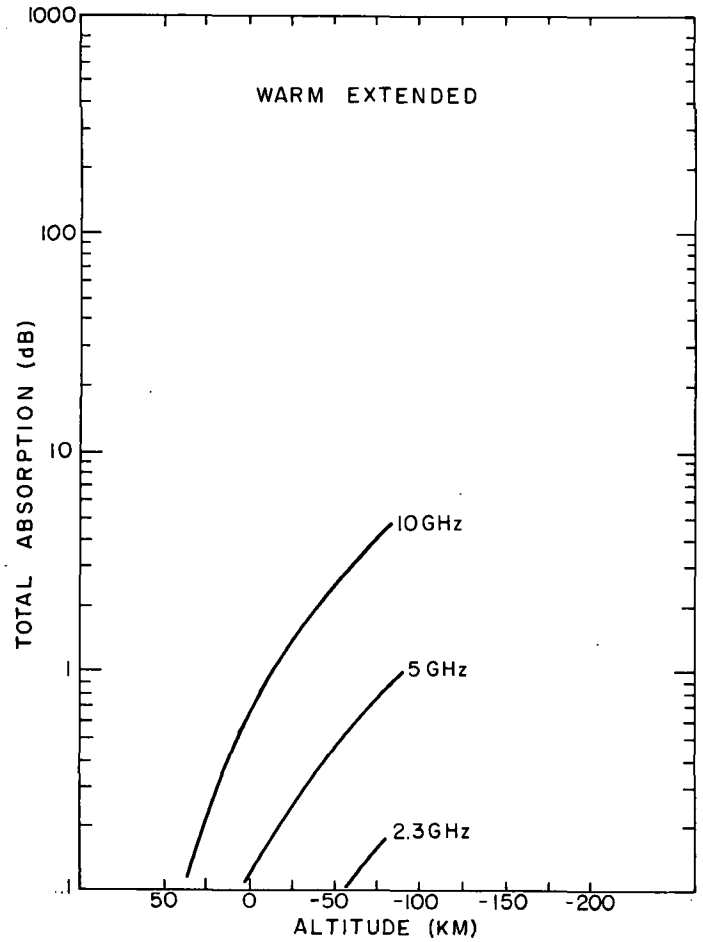

Figure 16. Total absorption vs. altitude for a signal propagating on a direct (radial) path calculated for the warm extended model Jovian atmosphere proposed by Lewis/JPL.

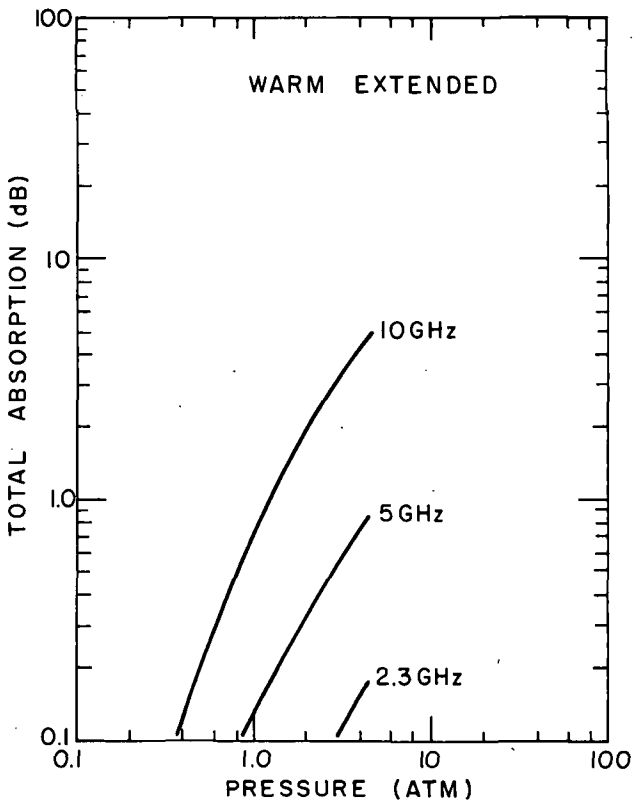

Figure 17. Total absorption vs. pressure for a signal propagating on a direct (radial) path calculated for the warm extended model Jovian atmosphere proposed by Lewis/JPL.

II. EFFECTS OF TURBULENCE IN JUPITER'S ATMOSPHERE

A. INTRODUCTION

We have until now postponed a discussion of the effects of atmospheric turbulence — if it occurs on Jupiter — upon 1 to 10 GHz frequency communication links. In the absence of any measured fluctuating quantity the uncertainties appeared too great. Moreover, a somewhat ad hoc planet-to-planet scaling law led to widely diverging results for Jupiter, depending on whether these were scaled to Earth or to Venus.

A numerical error in our first estimate of the permittivity variance appears to have yielded an incorrect scaling from Venus to Jupiter (ref. 3). Although the permittivity variance obtained after correction of this error then appears to be consistent with that obtained by scaling Earth values to Jupiter, we feel that the entire matter requires a careful discussion, particularly in view of the fact that no measurements in situ exist.

Also referring the reader to Section III of ref. 3, we will give a short introduction to the essentials of turbulence-induced fading.

Turbulence sets up a layer of "eddies" that can be regarded as nearly transparent lenses. In boundary-layer generated turbulence, the largest of these eddies have a size $L_o \propto z$, the altitude above the input boundary. The energy in these independently moving largest eddies is fully utilized in creating smaller eddies which move more or less independently inside the larger ones. A hierarchy of smaller eddies is thus set up, but there is a smallest size given by a microscale ℓ_o. These smallest eddies give up the energy transmitted to them in turn by larger ones to heat and friction. Each of these eddies contributes to δn the deviation from the average refractive index $\overline{n} \approx 1$.

In ref. 3, we showed that phase effects are governed by a path integral $\delta\phi(s)$ of the random quantity δn. Amplitude effects are governed by the amount of bending $\delta\theta$ of a ray from its original direction. This bending is properly described by another path integral over the transverse derivative of δn, provided diffraction effects are negligible. However, to exclude diffraction effects the point of observation must be well within the Fresnel zone (a cone of half-angle λ/ℓ for a scatterer of transverse size ℓ terminating a distance ℓ^2/λ beyond the scatterer) and also $\lambda << \ell$. When diffraction effects are negligible, and bending is very gradual, the variance of the phase builds up more rapidly than that of amplitude. In the limiting case of variations of δn *only* in the propagation direction there is no bending, therefore no amplitude changes but the phase shift $\delta\phi$ is non-zero, and its variance is proportional to $<(\delta n)^2>$ and to L, the pathlength. In the other limiting case that diffraction effects are all-important, the log-amplitude (i.e., the logarithm of the amplitude) has the same variance as the phase.

As far as variances are concerned, it appears that $<(\delta n)^2>$, ℓ_o, and L_o are the way the eddies enter into the problem. The importance of eddies of size ℓ is given by the way that $<(\delta n)^2>$ is built up out of their individual contributions. First of all, consider

$$<(\delta n)^2> = \int_o^\infty dK \; <[\delta n(K)]^2> \tag{11a}$$

where $\delta n(K)$ is the Fourier component of δn at wavenumber $k = \ell^{-1}$. Turbulence measurements indicate that

$$\text{(a)} \quad \langle [\delta n(K)]^2 \rangle \propto (KL_o)^2 \text{ for } KL_o << 1$$

$$\text{(b)} \quad \propto (KL_o)^{-5/3} \text{ for } L_o^{-1} \lesssim K << \ell_o^{-1}$$

$$\text{(c)} \quad \propto (KL_o)^{-5/3} \exp[-(K\ell_o)^2] \text{ for } K \gtrsim \ell_o^{-1}$$

This indicates that only those eddies with size ℓ such that $\ell_o << \ell \lesssim L_o$ are important for phase and amplitude effects. In all cases we consider, we have $L_o >> \lambda$. Although we do *not* necessarily have $\ell_o >> \lambda$, we see that certainly all effectively scattering eddies have size $\ell >> \lambda$ because $\ell >> \ell_o$. This is not completely true for amplitude effects, but we overstress this point to make clear that $\lambda << \ell$ for most eddies that contribute effectively to electromagnetic effects, i.e., the scattering angles are small. What this small-angle scattering does is to redistribute energy in a beam at a distance L, rather than to cause energy losses. A beam striking a small receiver (small compared to the local beamwidth) will not contribute less energy on the average to it: the received energy will fluctuate around a mean that is rather close to the free-space level. The signal will peak and it will fade at other times. Amplitude modulation is disturbed by both, and phase modulation particularly by the fades. One speaks of "signal fading" because one loses the message content during the times that rays are deflected away from the receiver such that the dips fall below the noise level.

The status of theory for the underlying amplitude effects which describe the fading, anno 1971, is not complete. The unfamiliar reader will have great difficulty discerning fact from fallacy in the existing literature. Therefore we give it in a nutshell:

The quantity that is measured is proportional to the square of the electric field. Be it a power or a flux; we call it I(t) and compare it to the steady-signal measure I_o observed in equivalent free-space conditions. The statistics of I(t) are governed by pathlength regimes.

1. $L > kL_o^2$, Diffraction Regime

Theory indicates that I(t) follows a Rice distribution. The electric field consists of a steady part with amplitude $E_o \exp(-\sigma_\epsilon^2)$ and a Gaussian part δE with zero mean and with variance $I_o [1-\exp(-2\sigma_\epsilon^2)]$. The quantity σ_ϵ^2 is given by Eq. (28) in Section II.D. Unfortunately, no measurements exist for $\sigma_\epsilon^2 > 1$. In particular, the variance of I, which we normalize as follows: $\sigma_I^2 = [\langle I^2 \rangle - \langle I \rangle^2] / \langle I \rangle^2$, is given as

$$\sigma_I^2 = 1 - \exp(-4\sigma_\epsilon^2) \tag{11b}$$

2. $kL_o^2 >> L > k\ell_o^2$, Optical Regime

This is the regime for optics at the Earth's surface — a well-studied regime. The theory is incomplete, but measurements indicate that I is log-normal, i.e., that the logarithm of I is Gaussian. Therefore, workers in optics look at $C_\ell^2 = \langle (\ln I)^2 \rangle - (\langle \ln I \rangle)^2$. For

log-normal I, the relationship between C_ℓ^2 and σ_I^2 is $C_\ell^2 = \ln(1 + \sigma_I^2)$. The quantity C_ℓ^2 has been measured for many situations. We translate the result for C_ℓ^2 into one for σ_I^2 according to this last relationship, and describe the measurements empirically by,

$$\sigma_I^2 \approx \left[1 - \exp(-4\sigma_\epsilon^2)\right]^{\prime} \left[1 + \beta\sigma_\epsilon^{-0.4}\right] \tag{11c}$$

where β is an unknown constant slightly larger than unity. The constant β appears to depend on wind velocity, wavelength, and perhaps other parameters: it is poorly understood. Uniform turbulence in this regime yields

$$\sigma_\epsilon^2 \approx 0.5\, k^{7/6} L^{11/6} L_o \langle(\delta n)^2\rangle$$

3. $4\sigma_\epsilon^2 << 1$, or $L << k\ell_o^2$: Weak-Scattering and Geometrical-Optics Regimes

If $4\sigma_\epsilon^2 << 1$ in case 1 , we have a *weak-scattering* limit and the probability distribution of I reduces to a constant very nearly I_o, and a very small Rayleigh component with variance $2\sigma_\epsilon^2 I_o$. If on the other hand, this holds in case 2) we have a *quasi-geometrical-optics limit* with log-normal $I = I_o \exp(2\psi)$, and $\langle \psi \rangle = 0, \langle \psi^2 \rangle \approx \sigma_\epsilon^2$. Finally, when $L << k\ell_o^2$, we have a true geometrical-optics limit, but σ_ϵ^2 is negligibly small and no appreciable σ_I occurs. When $4\sigma_\epsilon^2 << 1$ in cases 1 and 2, we observe,

$$\sigma_I^2 = 4\sigma_\epsilon^2 \tag{11d}$$

Radio links in planetary atmospheres fall exclusively under cases 1 and 2, but if the turbulence is sufficiently weak so that $4\sigma_\epsilon^2 \gtrsim 1$ there is a proper theory only for case 1, but we believe that Eq. (11b) is a reasonable approximation for case 2 when $\sigma_\epsilon^2 \gtrsim 5$. The regime $0.5 \lesssim \sigma_\epsilon^2 < 5$ is not well described in case 2 because β is unknown. The parameter σ_ϵ^2 is known as the *weak log-amplitude variance*. Its name is inspired by Eq. (11d) because the variance of lnA, the log-amplitude, is just one fourth of σ_I^2, and $\sigma_I^2 = 4\sigma_\epsilon^2$ in the weak-scattering regime.

Thus, to sum it up: the signal-power variance σ_I^2 (normalized to the square mean power) is a measurable quantity that describes the amount of signal fading. It is related, according to the present-day state of knowledge, to a universal variance parameter σ_ϵ^2 that is a function of $\epsilon^2 = 4\langle(\delta n)^2\rangle$, and of wavenumber k, pathlength L, as well as of diverse turbulence scale lengths. When fading is weak, we have $\sigma_I^2 = 4\sigma_\epsilon^2$. For stronger fading, Eqs. (11b) and (11c) hold. Our task is to compute σ_ϵ^2 for the Jovian atmosphere. We can then predict signal fading on hypothesized radio links.

B. STATEMENT OF THE PROBLEM OF SCALING

A form of σ_ϵ^2 under the assumption that $\epsilon^2(z)$ follows an exponential law is given in Eq. (42) of ref. 1. Regardless of that specific form, one must have knowledge of the scale-lengths of turbulence and of ϵ^2.

First, we discuss the variance parameter $\epsilon^2(z)$ of the dielectric permittivity $\bar{\varepsilon}(z)$. As implied by Eq. (1) of ref. 3,

$$\bar{\varepsilon}(z) = 1 + 2 \sum_j \beta_j \bar{p}_j(z)/T(z) \tag{12}$$

Note a factor 2 for conversion of refractive index into permittivity variation. We have retained the nomenclature of the previous reports, but in Eq. (12) we denote the altitude above the surface of the planet by z. The dependence of ε, p, and T upon latitude and longitude can be disregarded in the present context. Consider a temperature fluctuation at altitude z, giving rise to a variation in permittivity.

$$\delta\varepsilon(z) = -2 \sum_j \beta_j \bar{p}_j(z) \delta T(z)/T(z) \tag{13}$$

Such a temperature fluctuation may occur because a parcel of air from another altitude is displaced through turbulent motion to z. The pressure difference is eliminated very rapidly, hence no δp term in Eq. (13). The overbars in Eq. (13) (which we will not use explicitly further on) indicate the average value around which the fluctuation occurs. Eq. (13) can also be written

$$\delta\bar{\varepsilon}(z)/[\bar{\varepsilon}(z)-1] = -\delta T(z)/T(z) \tag{14}$$

We can also write the above ratio as a density ratio under the assumption of isobaric perfect-gas behavior (as we have done in ref. 1, p. 44), but it is preferable to regard temperature fluctuations because these have been investigated by atmospheric workers (ref. 4). The spatial frequency (= wavenumber) content of $\delta\bar{\varepsilon}(z)$ is thus given by that of $\delta T(z)$. Workers in atmospheric turbulence attempt to measure a quantity such as

$$< [T(z+\vec{r}) - T(z)]^2 > \tag{15}$$

for a given spacing $\vec{r}$ and altitude z (the averaging is over time). Turbulence theory predicts that when $\ell_o < |\vec{r}| < L_o$ (i.e., when $|\vec{r}|$ is sandwiched between microscales and macroscales of turbulence) the above quantity is proportional to $r^{2/3}$. The constant of proportionality, C_T^2, is known as the *temperature structure constant*, and it can be a function of altitude z. Under certain circumstances (one speaks of *homogeneous turbulence*) $C_T^2(z)$ will be a reproducible constant when the averaging time is neither too short nor too long. Therefore a body of theory has been worked out for $C_T^2(z)$. From the $r^{2/3}$ theory and its extension outside the turbulence scales it can be shown (ref. 5) that

$$< (\delta T)^2 > \approx 2.08\, C_T^2\, L_o^{2/3} \tag{16}$$

Consequently, we apply this to the mean square of Eq. (14) to obtain:

$$\eta^2(z) \equiv \epsilon^2(z)/[\bar{\varepsilon}(z)-1]^2 = 2.08\, C_T^2\, L_o^{2/3}/T^2 \tag{17}$$

(C_T, T, and perhaps L_o are functions of z)

The quantity $\eta(z)$ is the one we wish to scale from planet to planet. To do so we must decide what altitude dependence it has on each planet, and also to what extent $C_T L_o^{1/3}/T$ depends upon the planet.

C. CONCLUSIONS FROM TURBULENCE THEORY

In the following, we extract from material recently accumulated by Wyngaard, Izumi, and Collins, Jr. (ref. 6):

A large body of flow data indicates that under conditions of homogeneous turbulence

$$C_T^2(z) = 3.2\, N \varepsilon^{-1/3} \tag{18}$$

ε: rate of turbulent kinetic energy dissipation in $m^2 s^{-3}$
$N(z)$: rate of destruction of $< (\delta T)^2 > /2$ in $(^\circ K)^2 s^{-1}$.

Gurvich (ref. 7) has recently utilized atmospheric-circulation estimates by Golitsyn (ref. 8) giving ε to obtain estimates of $N(z)$ and ε for Venus. The drawbacks of his approach are: (a) that the altitude dependence of $C_T(z)$ is not given clearly, (b) that the calculation of ε is derived from the assumption that solar energy is the sole source of ε (this assumption is probably not correct for Jupiter). At present, we therefore prefer not to follow this approach.

Turbulence similarity theory, supported by many measurements, indicates that the combination

$$C_T^2(z) z^{-4/3} (\partial \bar{\theta}/\partial z)^{-2} \tag{19}$$

is a universal function of a parameter known as Richardson's number. Here, $\bar{\theta}$ is the average potential temperature, $\theta = T + \gamma_a z$ where γ_a is the ratio of gravitational acceleration g to specific heat c_p. Unfortunately, this still does not make explicit how C_T varies with z. Once again, the similarity hypothesis is invoked by introducing a reference temperature T_* at the input altitude of the turbulent layer (e.g., at the suface z = 0 for boundary-layer turbulence, and presumably also at an altitude $z > 0$ where a strong wind-shear effect creates a localized layer of turbulence), and a reference length L_*. The similarity theory predicts (and the prediction is verified again by measurement) that (ref. 6),

$$C_T^2(z) = T_*^2\, z^{2/3}\, g_3(z/L_*) \tag{20}$$

Under unstable conditions — those under which turbulence can be maintained — temperature decreases with increasing z and L_* is negative. For those conditions

$$g_3 = 4.9\,(1 - 7z/L_*)^{-2/3} \tag{21}$$

Equations (20) and (21) provide the explicit dependence of $\eta(z)$ upon z, when inserted into Eq. (17). Thus,

$$\eta^2(z) = 2.08\,(T_*/T)^2\,(z/L_o)^{-2/3}\,g_3(z/L_*) \qquad (22)$$

is the scaling factor for the permittivity standard deviation (squared) when a shear wind induces turbulence in a layer above z = 0. The reference quantities T_* and L_* are *not* functions of z.

In ref. 7. Gurvich assumes $L_o = az$, citing numerous measurements bearing out this assumption and yielding $a \approx 2.5$ Can this assumption also be "justified"? The following argument suggests that it can: temperature fluctuations at altitude z are caused by swift transport of parcels of air of temperature T(0) at z = 0 to the new altitude z. At altitude z, the local temperature fluctuation $\delta T \lesssim T(0)-T(z)$ due to mixing of air from the lower layer with ambient air. Therefore $<(\delta T)^2> \lesssim <[T(0)-T(z)]^2>$. The righthand side of this inequality corresponds to a "structure function" of temperature at altitude z measured with constant spacing z, e.g., as in Eq. (15), and consequently we set it proportional to $(z)^{2/3}$. The comparison with Eq. (16) then suggests $L_o = az$. With this simplification, Eq. (22) can be written as

$$\eta^2(z) \sim (T_*/T)^2\,g_3\,(z/L_*) \qquad (23)$$

Thus, the scaling of $\eta(z)$ from planet to planet is given by the ratio T_*/T. The factor $g_3(z/L_*)$ approaches a constant 4.9 as $z/|L_*| \to 0$, see Eq. (21), and we need take this factor into consideration only for altitude dependence of $\eta(z)$ once we have determined the maximal value given by the ratio T_*/T.

Unfortunately, T_* in general appears to be determined by the input mechanism of the turbulence — an unpredictable quantity. However, for near-adiabatic conditions under which wind and temperature gradients are similar, Tatarski (ref. 9) indicates a relationship for the mean potential temperature $\theta(z)$,

$$\theta(z) = \text{const.} + T_*\,\ln(z/z_s) \qquad (24)$$

where z_s is a surface roughness length. The result for $\eta(z)$ is obtained by substituting $T_* = z\partial\theta/\partial z$ [from Eq. (24)] into Eq. (23).

$$\eta^2(z) \sim |z\partial\theta/T\partial z|^2\,g_3(\Delta z/L_*) \qquad (25)$$

Under very unstable conditions, i.e. $\partial\theta/\partial z$ much less than zero, one finds L_* on Earth to be not more than several tens of meters. Greater instability leads to smaller L_*. Because $\epsilon(z)$ scales with altitude as $[\bar{\epsilon}(z)-1]\eta(z)$, and because the first of these factors scales as exp(-z/h) where h is a scale height of at least 5 km, we note that turbulence is restricted in this case to a thin layer of extent L_* [because $\eta(z)$ scales with $g_3(z/L_*)$]. Applying

Eq. (42) of ref. 1 or any similar equation, we note that $\sigma_\epsilon(z)$ is determined by $\epsilon_1^2(z)L_*$. Admittedly, $\epsilon_1^2(z)$ will be higher than predicted by Eq. (25).

Under slightly unstable conditions, L_* will be large, increasing as $\partial\theta/\partial z \to 0$. While $\eta(z)$ may then decrease at any altitude z, L_* may become so large that $\epsilon(z)$ scales with altitude as $[\overline{\varepsilon}(z)-1]$, i.e., as exp(-z/h), and consequently $\sigma_\epsilon(z)$ will be determined by $\epsilon_2^2(z)h$ (for a vertical path). Here, $\epsilon_2^2(z)$ is determined by Eq. (25).

The following contrasting situation has thus been obtained: under very unstable conditions we find $\sigma_\epsilon \sim \epsilon_1^2 L_*$, and under slight deviations from stability, $\sigma_\epsilon \sim \epsilon_2^2 h$. We have $L_* \sim 0$ in one limit, and $\epsilon_2^2 \to 0$ in the other. In one limit, the turbulence is restricted to too thin a layer to be felt, and in the other limit it is quenched: in both cases $\sigma_\epsilon \to 0$. Nevertheless, it appears to us that wide layers of slightly unstable conditions will be felt most severely with respect to turbulence-induced signal fading in the upper atmosphere of a planet. The gradual increase in signal fading noted by Venera 4 (ref. 10) appears to indicate that σ_ϵ is not determined by a thin layer. Furthermore, let us consider the factor $|z\partial\theta/T\partial z|$ in Eq. (25). Under near-stable conditions, $\theta(z) = T(z)-\gamma_a z$ has only a very weak dependence on z. On Earth and Venus $\gamma_a \sim 10^{-2}$ °K/m, on Jupiter perhaps $\gamma_a \sim 3 \times 10^{-2}$ °K/m. Under slightly unstable conditions we presumably have $\partial\theta/\partial z << \gamma_a$. Consequently we observe that

$$\eta(z) << \gamma_a z/T(z) \tag{26}$$

for turbulence in a wide planetary atmospheric layer. Let us see what inferences can be drawn for Earth and Venus.

1. *Earth*. Tropospheric measurements at altitudes 1.5 km $< z \leq$ 8 km indicate values of ϵ that do not exceed 1.5×10^{-6}. There are many indications that $\epsilon(z)$ will decrease with altitude. Because $\overline{\varepsilon}(z)-1$ also decreases with altitude it may be that $\eta(z)$ will not vary strongly with altitude. There is a difficulty in assigning a "direct" value to $\eta(z)$ by computing $\epsilon(z)/[\overline{\varepsilon}(z)-1]$, because we do not know at which altitude $\epsilon = 1.5 \times 10^{-6}$. However, $2.5 \times 10^{-4} < [\overline{\varepsilon}(z)-1] \lesssim 4.7 \times 10^{-4}$ in the troposphere, consequently our "direct" value for $\eta(z)$ is $3 \times 10^{-3} \lesssim \eta < 6 \times 10^{-3}$ as well as can be determined at present. This is quite consistent with Eq. (26) which predicts $0.05 < \gamma_a z/T < 0.25$ at these altitudes.

2. *Venus*. Unfortunately many less data are available for this planet. As set forth at the end of Section V.B of ref. 1, we have found a value $\epsilon \sim 6 \times 10^{-5}$ at $z \sim 20$ km under the assumption that $\epsilon(z)$ scales with exp(-z/h). However, that value has been obtained under the assumption of a fixed macroscale of turbulence. Utilizing the theory developed in Section II. D. of this report where we assume $L_o = az$, we find a new estimate $\epsilon \gtrsim 10^{-4}$ at $z \sim 20$ km. From diverse sources, e.g., Yakovlev and Yakovleva (ref. 10), we obtain $\overline{\varepsilon} - 1 \sim 1.7 \times 10^{-2}$ at this altitude (one must remember to correct the altitude scale in ref. 11). The ratio of these estimates yields $\eta \gtrsim 5 \times 10^{-3}$. There are indications from Venus too (see Kolosov, et al., ref. 10, Table 1) that C_n, hence ϵ, decreases with altitude, and that η therefore may not vary strongly with altitude.

The above considerations seem to indicate that $\eta(z)$ is not a strong function of altitude within a scale height. Moreover, the estimates $3 \times 10^{-3} < \eta < 6 \times 10^{-3}$ for Earth and

$\eta \gtrsim 5 \times 10^{-3}$ for Venus are not far apart. This appears to imply that η is a universal value, i.e., that for wide-layer turbulence one expects values of η that do not exceed a maximal value somewhere between 10^{-3} and 10^{-2}. We are inclined to postulate as working hypothesis that worst-case conditions yield $\eta \sim 6 \times 10^{-3}$ on Jupiter — an intermediate value. This value may be wrong by a factor 2 or 3, but we do not see how to obtain more accurate estimates.

We have thus argued that planetary turbulence must occur in wide layers in order to affect communications significantly, at least in principle. In order for wide layers of turbulence to be maintained one must have a temperature profile very close to the adiabatic, with negative potential temperature gradient. In that case, we argued, the ratio of standard deviation to average permittivity deviation, η will be much less than $\gamma_a \Delta z/T$ where Δz is the height above the reference altitude. We observed that this is consistently the case on Earth and Venus. We also observed that, in general, we can only find $\eta(z) < T_*/T$, but we cannot estimate T_*. Therefore, we turned to the data to find that η does not differ from Earth to Venus, nor does it vary appreciably with altitude. We have therefore assumed as a useful working hypothesis that $\eta \sim 6 \times 10^{-3}$ at the boundary layer of turbulence on Jupiter, Venus, and Earth (this value appears to be within a factor 2 for the two known cases) and thus find

$$\epsilon(z) \lesssim 6 \times 10^{-3} \, [\bar{\varepsilon}(z) - 1] \tag{27}$$

D. WEAK LOG-AMPLITUDE VARIANCE FOR SLANT-PATH LINKS

Although we now have an estimate for ϵ^2, we believe that a credible calculation of the weak log-amplitude variance σ_ϵ^2 is very hard to give in the absence of measurements. Consider slant-path propagation at an angle θ with the local normal from an altitude z_o to Earth (i.e., to infinity). The most general expression for σ_ϵ^2 is given in ref. 12 (where this quantity is dubbed $< B_r^2 >$). Adopting Eq. (8a) of ref. 12 to our case, we have

$$\sigma_\epsilon^2 = \frac{k^2}{16\pi} \int_{s_o}^{\infty} ds \, \epsilon^2(z) \int_0^{\infty} dK K \Phi(K) \, [1 - \cos(K^2 \Delta s/k)] \tag{28}$$

where s (or $\Delta s = s - s_o$) is the path parameter (i.e., $s = z/\cos\theta$). The use of this expression is fraught with difficulties. First of all, the path parameter s is confined to the layers of turbulence, e.g., to where $\epsilon^2(z) \neq 0$. We have seen in Section II.C [Eqs. (21), (26)] that

$$\epsilon^2(z) = \epsilon^2(0) e^{-2z/h} (1 + 7z/L_*)^{-2/3}$$
$$\epsilon(0) = \eta \, [\bar{\varepsilon}(0) - 1] \tag{29}$$
(we replace $-L_*$ by L_* for convenience)

in a layer starting at altitude z = 0. There may be several such layers (with different L_*), z_o (= $s_o \cos\theta$) may lie above or below z = 0, and L_* may be larger and smaller than h. Each of these possibilities affects the evaluation of Eq. (28) in a different way.

A second set of difficulties is introduced in specifying the refractive-index spectrum (ref. 3) $\Phi(K) = 15.7\, L_o^3\, (1+K^2L_o^2)^{-11/6}$. The frequency dependence of σ_ϵ^2 is determined by whether or not the factor $[1-\cos K^2 \Delta s/h]$ alters the integrand $K\Phi(K)$ in Eq. (28) appreciably. If $(s/k)^{1/2} \ll L_o$, then one finds $\sigma_\epsilon^2 \propto k^{7/6}$. If $(s/k)^{1/2} >> L_o$ then $\sigma_\epsilon^2 \propto k^2$. However, the effective length of $(s/k)^{1/2}$ depends both on the location of the layer with respect to z_o, and upon its thickness. Furthermore, the outer scale L_o is observed to be proportional to z, therefore it is not constant.

Boundary-layer turbulence on Earth appears to indicate that L_* is much less than scale-height h. The Hufnagel curve (ref. 13) for sunny day turbulence follows a $C_n^2(z) \propto z^{-4/3}$ law; this corresponds in Eq. (29) with $L_* << h$. At the same time, the dependence $L_o(z) = az$ appears to hold up to heights that are an appreciable fraction (say 0.2) of the scaleheight h.

Let us compare $L_o = a(z_o + \Delta z)$ to the length $(\Delta z/k\cos\theta)^{1/2}$. With $a \approx 2$, and $k\cos\theta >> 1$ in the 1 to 10 GHz frequency range, we observe that L_o is certainly the larger of these two lengths (for not-too-large angles). The spectral function $\Phi(K)$ may therefore be approximated in Eq. (28) by $15.7\, L_o^{-2/3} K^{-11/3}$, i.e.,

$$\sigma_\epsilon^2 = \frac{15.7\, k^2}{16\pi \cos\theta} \int_{z_o}^{\infty} dz \epsilon^2(z)(az)^{-2/3} \int_o^{\infty} dK K^{-8/3} [1 - \cos(K^2 \Delta z/k\cos\theta)] \quad (30)$$

The dK integral can be transformed into a number by transforming K to the new variable $q = K^2 \Delta z/k\cos\theta$. The number is

$$\int_o^{\infty} dq\, q^{-11/16} (1 - \cos q) \approx 1.65.$$

The resulting expression for σ_ϵ^2 becomes,

$$\sigma_\epsilon^2 \approx 0.2\, k^{7/6} a^{-2/3} (\cos\theta)^{-11/6} \int_{z_o}^{\infty} dz \epsilon^2(z)(\Delta z)^{5/6} z^{-2/3}. \quad (31)$$

The numerical constant is obtained by approximating $15.7 \times 1.65/32\pi \approx 0.2$. We have yet to evaluate the remaining integral. That is, we must evaluate

$$\epsilon^2(0) \int_{z_o}^{\infty} dz\, z^{-2/3} (1 + 7z/L_*)^{-2/3} (\Delta z)^{5/6} \exp(-z/h). \quad (32)$$

Strictly speaking, the above integral is valid only for $z_o \geqslant 0$. Equation (28) is different when $z_o < 0$. Consider, first of all, that the probe is in the turbulent layer, i.e., $z_o \geqslant 0$. Because the integrand converges to zero as $\Delta z \to 0$, even for $z_o = 0$, we may assume $7z/L_* >> 1$ in the integrand to obtain,

$$7^{-2/3} L_*^{2/3} h^{1/2} \epsilon^2(0) e^{-z_o/h} \int_o^\infty dx (x + z_o/h)^{-4/3} x^{5/6} \exp(-x). \tag{33}$$

Although the opposite limit can also be calculated, we can set $z_o << h$ to find a "worst" case. We can then drop all terms proportional to z_o/h to obtain

$$\sigma_\epsilon^2 \approx 0.1\, a^{-2/3} k^{7/6} L_*^{2/3} h^{1/2} \epsilon^2 (\cos\theta)^{-11/6}. \tag{34}$$

The numerical estimate of this quantity requires several auxiliary estimates. On Earth, boundary-layer turbulence measurements yield $1.5 < a < 2.5$. On Earth, also, $L_* \sim 10$m on sunny days with well-developed turbulence. We do not know how large L_* can become, but it is hard to conceive of L_* exceeding the scaleheight h. Finally let us assume a "worst" case layer starting at the p = 4 atm height, i.e., close to the cloud layer. In Fig. 18, we have plotted $\epsilon = \eta(\bar{\epsilon}-1)$ vs altitude or pressure of a hypothesized boundary layer for the three "Lewis-JPL" models of Jovian refractivity. Utilizing this graph to set $\epsilon \lesssim 7 \times 10^{-6}$, we observe that $(kh)^{7/6} \sim 4 \times 10^6$ at 1 GHz so that with a = 2 we obtain

$$\sigma_I^2 = 4\sigma_\epsilon^2 \lesssim 4 \times 10^{-5} (\cos\theta)^{-11/6} (f/f_{1\ GHz})^{7/6} \tag{35}$$

It is quite clear that $\sigma_I^2 = 4\,\sigma_\epsilon^2$ represents a very weak signal-power variance more than 30 dB below the square mean power for frequencies less than 10 GHz. Only when $\cos\theta << 1$, i.e., for occultation angles, are matters different, but in that case the whole calculation breaks down. We will regard it separately.

It is also possible to allow z_o to be negative, i.e., to have a layer of turbulence far above the probe. In this case it is possible that the cosine term in Eq. (28) does not contribute, namely when the distance $(s_o/k)^{1/2} > K_o$. Here, s_o is the distance from the probe to the boundary layer. This is conceivable only for thin layers, and instead of $(kh)^{7/6}$ we would get something like $k^2 dL_o$ with $d << h$, $L_o << h$. The ratio is $(kh)^{5/6}(dL_o/h^2)$; obviously less than predicted by Eq. (34) with $L_* = h$.

In conclusion, we believe that these considerations, despite all of the above discussed uncertainties and approximations indicate that Jovian turbulence will not affect slant-path links in the 1 to 10 GHz frequency range with probes down to the cloud layer.

Footnote: We wish to apply Eq. (34) in recomputing ϵ^2 for the planet Venus, since it appears to us that this formula is more accurate than previous ones. The Russian Venera-4 data (ref. 3) yielded $\sigma_\epsilon^2 \sim 0.04$ and the reentry angle θ was such that $(\cos\theta)^{-11/6} \sim 4$. The frequency was 942 MHz, and h ~ 12.7 km. This yields

$$\bar{\epsilon}_{Venus} \sim 10^{-4} (h/L_*)^{1/3}$$

which thus suggests $\epsilon \gtrsim 10^{-4}$ on Venus at 20-km altitude. We have utilized this estimate in Section II.C. It compares reasonably well with the cruder estimate of ref. 1 (end of Section V.C.).

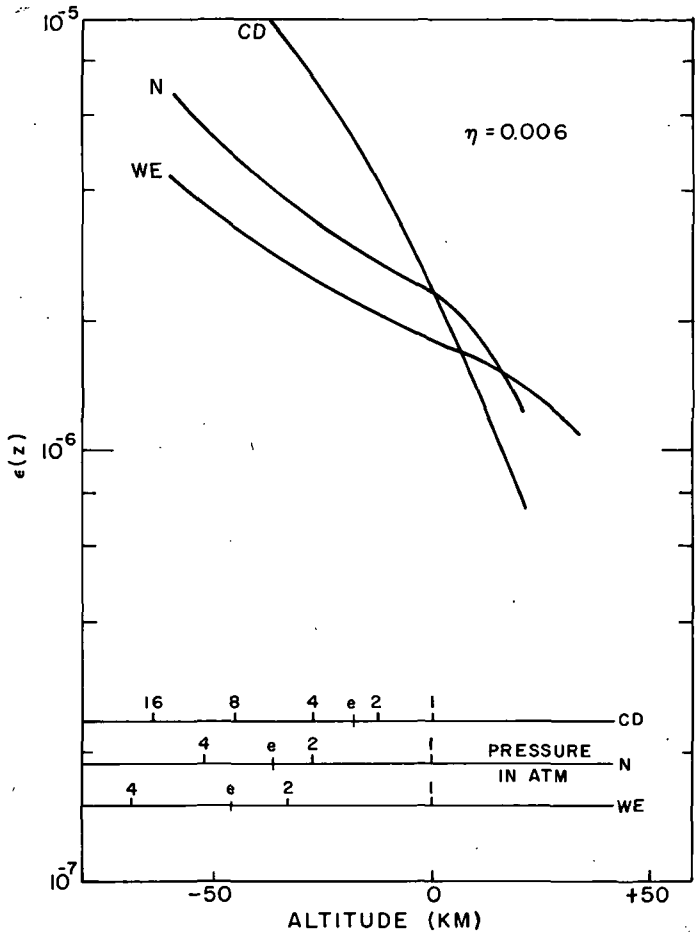

Figure 18. Estimated standard deviation of the dielectric permittivity of Jupiter's atmosphere for the cool-dense, nominal, and warm-extended models proposed by Lewis/JPL.

E. WEAK LOG-AMPLITUDE VARIANCE FOR OCCULTATION LINKS

The calculation of σ_ϵ^2 is governed by an equation similar to Eq. (28), only s is integrated from s = - ∞ to s = + ∞. The pathlength parameter is related to the height Δz above the altitude of closest approach z_o by the relationship $|s| \approx (2R\Delta z)^{1/2}$ which is in error by $0(z_o/R)$. Transforming to a z integral, we obtain

$$\sigma_\epsilon^2 = \frac{k^2}{16\pi}(2R)^{1/2}\int_{z_o}^{\infty} dz(\Delta z)^{-1/2}\epsilon^2(z)\int_0^{\infty} dK K\Phi(K)\left\{1-\cos\left[2R\Delta z)^{1/2}/k\right]\right\} \quad (36)$$

We must now attempt to work our way through the problems enumerated in the preceding section. Where possible, we will just retrace the succeeding steps and adapt them to Eq. (36). Again, let R include the altitude up to the initiation of turbulence, and let z_o be the relative altitude of closest approach ($z_o > 0$) we then compare $L_o = a(z_o + \Delta z)$ to $(2R\,\Delta\, z/k^2)^{11}$. At 1 GHz, and Δz = 10m, we find $(2R\,\Delta\, z/k^2)^{1/4} \approx 20$ m. At 10 GHz, this length is reduced by a factor 3. Therefore it again appears very reasonable to assume that L_o is the largest of these lengths. We follow the same step as in deriving Eqs. (31) from (30), to obtain

$$\sigma_\epsilon^2 = \frac{15.7 \times 1.65}{32\pi}\, a^{-2/3}(2R)^{11/12}k^{7/6}\epsilon^2(0) \times \int_{z_o}^{\infty} dz(\Delta z)^{-1/12}z^{-2/3}\,(1 + 7z/L_*)^{-2/3}e^{-z/h} \quad (37)$$

The integrand does *not* converge as $z \to z_o$, so additional care must be taken in making approximations.

(a) When $z_o << L_* << h$, it is clear that the integral in Eq. (37) is proportional to $L_*^{1/4}$

(b) For $L_* << z_o << h$, we obtain for the integral a value proportional to $L_*^{2/3}z_o^{-5/2}$.

With some numerical analysis, we observe that we really obtain for the integral

(a) $0.3\, L_*^{1/4}$ for $z_o << L_*$

(b) $0.9\, L_*^{2/3}z_o^{-5/12}$ for $L_* << z_o$

Thus, the following two cases are obtained:

$$\sigma_\epsilon^2 \sim 0.05\, k^{7/6}L_*^{1/4}(2R)^{11/12}\epsilon^2 \text{ for } z_o << L_*$$
$$\sim 0.15\, k^{7/8}L_*^{2/3}z_o^{-5/12}(2R)^{11/12}\epsilon^2 \exp(-2z_o/h) \text{ for } z_o > L_* \quad (38)$$

The larger of these estimates is the $z_o << L_*$ case, which we reorganize into

$$\sigma_\epsilon^2 \sim 0.05\, \epsilon^2\, (2kR)^{7/6}.\, (L_*/2R)^{1/4}$$

Note that the unknown length appears to the one-fourth power, so that a factor 10 error in L_* is not a severe error in σ_ϵ^2. Setting $L_* \sim 100$m, $R \sim 7 \times 10^7$m, $\epsilon \sim 7 \times 10^{-6}$ we obtain at 1 GHz, $\sigma_\epsilon^2 \sim 0.04$. Thus,

$$\sigma_I^2 \sim 0.15\, (f/f_{1\ GH_z})^{7/6} \tag{39}$$

It appears to us, unless we have grossly underestimated ϵ^2, that Eq. (39) is a reasonable estimate — the uncertainty in scalelengths that was a problem for slant paths is much less. If so, the above value of σ_I^2 indicates that at frequencies well below 10 GHz, occultation links grazing the cloud layer will also not experience appreciable fading (we bring to mind the fact that σ_I must exceed unity for appreciable fading). The above estimate must be reconsidered for higher frequencies because Eq. (39) then predicts marginal to strong fading. However, at f = 1 GHz, it is hard to jack up σ_I^2 to unity. For example, even if $L_* \sim$ h, a factor $\sim (20)^{1/4} \sim 2$ is not sufficient to do this. We note that either assuming a boundary layer at higher altitudes, or penetrating the layer of turbulence less deeply so that the second of Eqs. (38) holds, only serves to *lower* the above estimate.

Conclusion: At frequencies not exceeding 1 GHz greatly, turbulence will not affect occultation-pathlinks on Jupiter above the cloud layer. At higher frequencies its effect is eclipsed by absorption losses (which increase as f^2). The work of this section may entail modifications of previous work on Venusian atmospheric turbulence. Specifically, the fading curves of refs. 1 and 3 were based on Rice statistics. It now appears that the signal strength can fluctuate as a log-normal random variable. This stresses the importance of strong peak intensities (inverse fades) compared to the Rice-statistics governed case. Also, previous work did not utilize the present altitude-dependent model of C_n^2. While it is not anticipated that these modifications will cause great changes, future work should include a reinvestigation along these points.

III. NEW TECHNOLOGY APPENDIX

The work performed under this study contract has led to improved understanding of the communications medium. However, the very nature of this work — as in most study contracts — precludes technological innovations, and none have resulted in this Phase.

REFERENCES

1. J. W. Davenport and D. A. de Wolf, "Investigation of Line-of-Sight Propagation in Dense Atmosphere: Phase II", NASA CR-114288 (July 1971).

2. Private Comm. N. Divine, extract from monograph "The Planet Jupiter (1970)," Jet Propulsion Laboratory Report to NASA Ames Research Center (to appear in 1971).

3. D. A. de Wolf and J. W. Davenport, "Investigation of Line-of-Sight Propagation in Dense Atmosphere: Phase I," NASA CR-73440 (March 1969-May 1970).

4. J. L. Lumley and H. A. Panofsky, *The Structure of Atmospheric Turbulence*, (Interscience, J. Wiley & Sons, New York, 1964).

5. J. W. Strohbehn, Proc. IEEE **56**, 1301 (1968): (see p. 1303).

6. J. C. Wyngaard, Y. Izumi, and S. A. Collins, Jr., J. Opt. Soc. Am. **61**, 1646 (1971).

7. A. S. Gurvich, Fizika Atmosferi i Okeani **5**, 1172 (1969).

8. G. S. Golitsyn, Physics of Atmospheres and Oceans **4**, 651 (1968).

9. V. I. Tatarski, *Wave Propagation in a Turbulent Medium*, transl. R. A. Silverman (McGraw-Hill, New York 1961), p. 191. See also D. J. Portman, E. Ryznar, and A. A. Waqif, "Laser Scintillation Caused by Turbulence near the Ground", U. of Michigan Research Report 225 for USA CRREL (January 1968).

10. M. A. Kolosov, O. I. Yakovlev, G. D. Yakovleva, and A. I. Yefimov, "Radio-Wave Fluctuations and Refraction Coefficient Variations in the Venusian Atmosphere," COSPAR Meeting (paper m 23) Leningrad, May 22, 1970.

11. O. I. Yakovlev and G. D. Yakovleva, Radio Eng. & Electr. Phys. **14**, 503 (1969).

12. D. A. de Wolf, Radio Science **2**, 1513 (1967).

13. R. S. Lawrence and J. W. Strohbehn, Proc. IEEE **58**, 1523 (1970), Fig. 1 (the Hufnagel paper is not readily available).

APPENDIX I
DERIVATION OF SLANT-PATH ABSORPTION

Consider a slant path defined by the deepest penetration depth (R_o) as measured from the center of the planet and slant angle (Figure I-1). If the atmosphere has an absorption coefficient that decays exponentially with increasing altitude above the planet, then the total absorption along that slant path is given by Eq. (I-1)

$$I(R_o, \theta) = \int_{R_o \cos\theta}^{\infty} \alpha_o \exp\left[-(s^2 + d_o^2)^{1/2}/h\right] \qquad \text{(I-1)}$$

where $I(R_o, \theta)$ is the total absorption along the slant path defined by R_o and θ, and h is the scale height governing the decay of the absorption coefficient, $d_o = R_o \sin\theta$ is the impact parameter for the slant path, s is the distance as measured along the slant path starting from the point of closest approach, and $\alpha_o \exp(-R_o/h)$ is the absorption coefficient at the altitude R_o.

After the substitutions

$$z^2 = (s^2 + d_o^2)/h^2$$

and

$$b \equiv R_o/h$$

Eq. (I-2) is obtained.

$$I(R_o, \theta) = \alpha_o h \int_b^{\infty} dz\, e^{-z} \left[1-(b \sin\theta/z)^2\right]^{-1/2} \qquad \text{(I-2)}$$

We now proceed to obtain upper and lower bounds for Eq. (I-2). Since $z \geq b$, the integral may be overbounded by setting $b\sin\theta/z = \sin\theta$. Thus

$$I(R_o, \theta) < \alpha_o h \int_b^{\infty} \frac{e^{-z}\, dz}{\sqrt{1 - \sin^2\theta}} = \frac{h\alpha_o e^{-R_o/h}}{\cos\theta}$$

$$I(R_o, \theta) < I_d / \cos\theta$$

where $I_d = I(R_o, 0)$ is the absorption on the direct path.

The absorption may also be underbounded by a suitable approximation to the non-exponential part of the integrand in Eq. (I-2), namely f(z). As shown in Fig. (I-1), f(z) may be underbounded by the straight line segments which are tangent to the actual function. The lower bound to f(z) is defined by

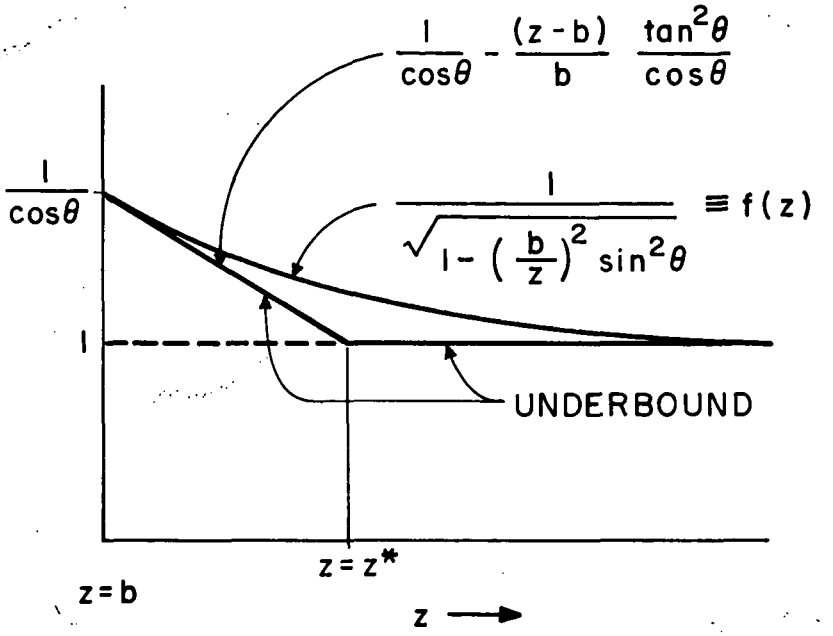

Figure I-1. Bounds on integrand for slant-path absorption calculations.

$$f_{1b}(z) = \frac{1}{\cos\theta} - \left(\frac{z-b}{b}\right)\frac{\tan^2\theta}{\cos\theta} \qquad b \leqslant z < z^* \qquad \text{(I-3)}$$

$$= 1 \qquad z \geqslant z^*$$

where

$$z^* = b\left(1 + \frac{1-\cos\theta}{\tan^2\theta}\right) .$$

After substitution of Eq. (I-3) into (I-2) and tedious but straight-forward algebraic manipulation, a lower bound to the slant parth absorption is obtained and is given by Eq. (I-4)

$$I(R_o,\theta) > \frac{\alpha\, e^{-b}\, h}{\cos\theta}\left(1 - \frac{\tan^2\theta}{b}\left[\left(1 - e^{-b(1-\cos\theta)/\tan^2\theta}\right)\right]\right) \qquad \text{(I-4)}$$

$$= \frac{I_{direct}}{\cos\theta}\,[1 - \text{correction}]$$

For Jupiter $b = R_o/h$ is a large number (greater than 1000) and the correction terms in Eq. (I-4) are negligible for slant angles below 85 degrees. Therefore the upper and lower bounds are extremely close to each other and the slant-path absorption for an exponential atmosphere may be taken to be $I_d/(\cos\theta)$.

The above approximation was derived for an exponential atmosphere. One does not require an exponential atmosphere for this approximation — only that curvature effects are small over an altitude range in which the absorption coefficient changes appreciably. Therefore, the derived approximation appears quite valid for the Jovian atmosphere.